MICROFLUIDIC ANALYSIS OF METASTATIC CANCER BIOMARKERS

A Dissertation

Presented to the Faculty of the Graduate School

of Cornell University

in Partial Fulfillment of the Requirements for the Degree of

Doctor of Philosophy

by

Steven Michael Santana

August 2014

MICROFLUIDIC ANALYSIS OF METASTATIC CANCER BIOMARKERS

Steven Michael Santana, Ph.D.

Cornell University 2014

Cancer is the second-leading cause of death in the United States. Metastasis is responsible for 90% of cancer-related death and progresses through multifarious, poorly-understood cascades as they are difficult to observe *in vivo*. It is widely held that deciphering the metastatic cascade and identifying metastatic precursors will lead to improved patient outcomes. In this work, we isolate and study cancer biomarkers, specifically circulating tumor cells (CTCs) and cancer-cell-derived extracellular shed vesicles (ESVs), implicated in cancer progression and metastasis. First we describe the design, fabrication, and use of a Hele-Shaw microfluidic system to optimize rare-cell immunocapture parameters with a focus on informing the design of systems for CTC isolation from patient whole blood. Our study includes the role of antibody selection, density, antigen locations, and multi-modal capture surfaces, as well as shear stress, on rare cell capture. We use LNCaPs, a PSMA-expressing prostate cancer cell line, as a model for CTCs and anti-PSMA antibodies, J591 and J415, to inform chemistry-mediated immobilization. Next, we focus on another cancer-disseminated marker, extracellular shed vesicles. ESVs, including exosomes and cancer-cell-derived microvesicles, are disseminated throughout the body and represent an important conduit of cell communication. Microvesicles have potential as a cancer biomarker as they are believed to transform tumor microenvironments and prime the metastatic niche. Cancer-cell-derived ESV subpopulations consist of a small-diameter exosome population and a large-diameter, cancer-cell-specific microvesicle population, each formed by unique mechanisms. It is believed that size correlates with biological properties of interest, but

isolating these subpopulations, to discern chemical, biological, or physical differences, is challenging. We designed a deterministic lateral displacement microfluidic platform to isolate a pure microvesicle sample from the heterogeneous cancer-cell-derived ESV population. The threshold diameter differentiating the microvesicle population from the exosome population was determined by characterizing the size distributions of ESVs harvested from multiple cancer cell lines of breast, brain, and pancreas origin. Our microvesicle-isolation microfluidic technology facilitates future investigations regarding microvesicles' role in cancer progression by enabling identification of cargo carried by the microvesicle subpopulation.

BIOGRAPHICAL SKETCH

Cornell University, Sibley School of Mechanical and Aerospace Engineering.

Master of Science in Mechanical Engineering, May 2014.

Adviser: Brian J. Kirby

Loyola Marymount University, School of Education.

Master of Arts in Education, December 2007.

Harvey Mudd College, Department of Engineering.

Bachelor of Science in Engineering, May 2006.

ACKNOWLEDGEMENTS

This work is dedicated to my family. To my wife, Kate; to my daughters, Madeleine and Charlotte; to my parents, Michael and Holly; and to my siblings, Samantha, Brett, Jaime, James, and Dannah. I thank them all for their love and support.

I am grateful to my advisor, Prof. Brian Kirby, for his efforts in mentoring and training me.

I also thank professors Richard Cerione, Claudia Fischbach, and John Sipple for serving on my thesis committee and Dr. Marc Antonyak who has provided much support and helpful conversation.

Finally I thank my colleagues who have been members of Prof. Kirby's research group: Jason Gleghorn, Benjamin Hawkins, Sowmya Kondapalli, Vishal Tandon, Alexander Barbati, Erica Pratt, Chao (Charlie) Huang, James Smith, Michael Bono, Fredrik Thege, Timothy Lannin, Marie Godla, and John (Jack) Hartman.

My work has been funded by the Alfred P. Sloan Foundation, NACME, the National Cancer Institutes under Award Number U54CA143876, and the National Science Foundation GK-12 Program under Award Number 0841291. A portion of my work was completed in the Cornell Nanoscale Science and Technology Facility (CNF) and the Cornell Nanobiotechnology Center (NBTC).

TABLE OF CONTENTS

LIST OF FIGURES

CHAPTER 1

INTRODUCTION

Cancer is the second-leading cause of death in the United States. Metastasis is responsible for 90% of cancer-related death (1, 2) and progresses through multifarious cascades that are poorly understood as they are difficult to observe *in vivo*. It is widely held that deciphering the metastatic cascade and identifying metastatic lesion precursors will lead to improved patient outcomes.

Cancerous epithelial tumors, or carcinomas, disseminate oncogenic cells that are thought to establish metastatic lesions and to sustain tumor growth. These tumor cells are delivered by lymphatic, hematogenous, and transcoelomic dissemination (3) and have potential to establish metastatic lesions. Circulating tumor cells (CTCs), the hematogenously distributed population, represent an accessible, noninvasive patient-derived sample of cancer cells (4–6) which are thought to establish metastatic lesions (7–9). CTCs have demonstrated usefulness as a prognostic indicator of survival (10–12), a biomarker for drug-target engagement (4, 13, 14), a measure of tumor-associated genomic instability (15–18), and a means of early disease detection (9, 19). Circulating tumor cells (CTCs), a putatively metastatic cell subpopulation, are an especially appealing cell source for studying cancer progression and metastasis in that they are readily accessible and can be noninvasively obtained from a peripheral blood draw.

In addition to disseminating metastatic cells, cancerous epithelial cells release extracellular shed vesicles (ESVs) into their local environment and throughout the body (20–26). ESVs contain multiple factors including proteins, mRNAs, miRNAs, RNA transcripts and enzymes (22, 27–35). ESVs, especially cancer-cell-derived microvesicles (MVs), represent a unique form of cell communication wherein vesicle uptake can induce a change in the recipient cell's behavior and function (2, 36, 37). Cancer-cell-derived ESVs are believed to sustain and promote growth in the primary

tumor and to prepare metastatic lesion microenvironments for tumor establishment and growth thereafter (38, 39) by sharing information and dysregulated programs among all cell types (21, 33, 40, 41).

Both cancer-disseminated populations, CTCs and MVs, are implicated in establishing and sustaining the tumor micronenvironment and the metastatic niche.

In this thesis, I describe the use of microfluidic devices to empirically parameterize CTC and rare-cell immunocapture devices and to isolate cancer-cell-derived MVs from a sample containing a heterogeneous ESV population. I also describe the physical and chemical characterization of cancer-cell-derived ESVs. In chapter 2, I present the implementation of a Hele-Shaw flow cell to define parameters, including antibody selection, density, antigen locations, and multi-modal capture surfaces, as well as fluid mechanical properties, to enhance the isolation of target rare cells, such as CTCs, in immunocapture microdevices. Given CTC rarity, immunocapture devices must be well tuned to optimize total capture efficiency. Chapters 3 and 4 describe cancer-cell-derived ESV characterization and the microfluidic isolation of MVs from a heterogeneous ESV population. Although ESVs have been interrogated for cargo, details regarding their provenance, shedding, uptake, and function are not well understood. This results, in part, from the bulk characterization of heterogeneous ESV samples. In chapter 3, I characterize the size distributions of ESVs shed from a number of cancerous epithelial cells, from multiple organs; I also identified cancer cells' dependence on glutamine metabolism for MV production. Using the ESV size distribution information, reported in chapter 3, I present, in chapter 4, a novel microfluidic device for the isolation of MVs from a heterogeneous ESV population contained within cancer-cell conditioned medium. This technology enables identification of cargo carried by the microvesicle subpopulation and future investigations regarding microvesicles' role in cancer progression.

I also contributed to a number of works (4, 9, 42–45) not discussed within this document. In Kirby, et al. (4), I conceived of and designed experiments for characterizing cell capture within immunocapture microfluidic devices, developed analysis tools, and analyzed data. In Smith, et al. (42), I wrote the section entitled *Engineering parameters that affect cell adhesion*. In Huang, et al. (43), I provided data analysis tools, a framework for experimental design, and advice regarding on-going experiments. In Rhim, et al. (9), I conducted experiments to isolate circulating epithelial cells from patient blood. In Smith, et al. (44), I provided experimental cell-adhesion data that informed rare cell capture prediction models. In Galletti, et al. (45), I provided training and support regarding the use of microfluidic devices for rare cell capture experiments.

CHAPTER 2

IMMUNOCAPTURE OF PROSTATE CANCER CELLS WITH ANTI-PSMA ANTIBODIES IN MICRODEVICES

2.1 Abstract

Patients suffering from cancer can shed tumor cells into the bloodstream, leading to one of the most important mechanisms of metastasis. As such, the capture of these cells is of great interest. Circulating tumor cells are typically extracted from circulation through positive selection with the epithelial cell-adhesion molecule (EpCAM), leading to currently unknown biases when cells are undergoing epithelial-to-mesenchymal transition. For prostate cancer, prostate-specific membrane antigen (PSMA) presents a compelling target for immunocapture, as PSMA levels increase in higher-grade cancers and metastatic disease and are specific to the prostate epithelium. This study uses monoclonal antibodies J591 and J415–antibodies that are highly specific for intact extracellular domains of PSMA on live cells–in microfluidic devices for the capture of LNCaPs, a PSMA-expressing immortalized prostate cancer cell line, over a range of concentrations and shear stresses relevant to immunocapture. Our results show that J591 outperforms J415 and a mix of the two for prostate cancer capture, and that capture performance saturates following incubation with antibody concentrations of $10\,\mu g\,mL^{-1}$.

The content of this chapter was submitted and published as a research article that is reproduced here with permission from *Biomedical Microdevices*. The article is titled: "**Immunocapture of Prostate Cancer Cells with Anti-PSMA Antibodies in Microdevices**" (46). DOI: 10.1007/s10544-011-9616-5. Authors include: Steven M. Santana (SMS), He Liu (HE), Neil H. Bander (NHB), Jason P. Gleghorn (JPG), and Brian J. Kirby (BJK). Author contributions are as follows: conceived and designed experiments (SMS, JPG, BJK), performed experiments (SMS), analyzed the data (SMS), provided antibodies (HE, NHB), wrote the paper (SMS), edited the paper (SMS, BJK).

2.2 Introduction

Patients suffering from metastatic prostate cancer (PCa) often shed tumor cells, called prostate circulating tumor cells (PCTCs), into the bloodstream (10, 47). While these PCTCs are rare and are outnumbered by as much as 10^9 hematologic cells per PCTC in blood, it is believed that these circulating tumor cells (CTCs) contribute to metastatic progression (48). PCTC enumeration has been shown clinically to be a valid prognostic indicator of patient survival (10, 11, 49). The capture of PCTCs may enable early clinical assessment of metastatic processes and chemotherapeutic responses, as well as genetic and pharmacological evaluation of cancer cells.

CTC isolation is inhibited by the uncertainty in defining appropriate enrichment schemes. Circulating nucleated cells (DAPI+) that show evidence of an epithelial history (EpCAM+, cytokeratin+) and are distinct (CD45-) from leukocytes are often classified as originating from the primary tumor and being related to metastasis (47, 50). Use of these identifying characteristics is supported by statistical observations that high counts of CTCs defined in this fashion correlate with poor prognosis (50). CTCs are most commonly extracted from circulation through an enrichment process by positive selection with EpCAM (also called CD326), a pan-epithelial marker (5, 12, 51, 52); this mechanism is employed by the CellSearch^{TM} system and by other immunocapture systems (6, 7, 10–12, 53).

EpCAM has often been selected as the target transmembrane protein in immunocapture systems because of the epithelial origin of the cells of interest, but this approach may introduce biases due to the dynamic nature of EpCAM expression in circulating cells (7). Importantly, patients with solid tumors and high CTC counts (as measured following

EpCAM enrichment) have poor prognoses (10–12, 50, 54, 55). Whereas EpCAM has been reported to correlate with invasiveness (56), indicate oncogenic potential (57), and be upregulated and correlate with proliferation in cell lines (58), the role of EpCAM in metastatic cancer is unclear. An important cellular phenotype change, epithelial-to-mesenchymal transition (EMT), characteristic of many invading cancer cells results in a cells loss of epithelial characteristics. This transition may cause some populations of CTCs to avoid extraction through epithelial-based (anti-EpCAM) capture techniques as EpCAM expression (7, 8) does not correlate with EMT markers (59). Furthermore, markers expressed after EMT may be more important in predicting cancer progression as they contribute to metastatic potential (60). EMT has been reported to increase a cell's ability to become invasive, perhaps leading to a higher probability of tumorigenicity; thus, cells more aggressive in the generation of new tumors might not be isolated by EpCAM enrichment (7).

In prostate tissues, including PCTCs, prostate-specific membrane antigen (PSMA; also know as: folate hydrolase 1; glutamate carboxypeptidase II), a type II transmembrane metallopeptidase, is a well-established ligand that is accessible to antibodies (61–64). Virtually all prostate cancer primary tumors express PSMA (65–68), whereas PSMA expressed in prostate vascular endothelium of benign tissue (69). PSMA levels increase progressively in higher-grade cancers, metastatic disease, hormone-refractory cancer, progressing cancer, and cancers exhibiting rising blood PSA following prostatectomy (65, 70–75). Thus, anti-PSMA immunocapture is likely to capture circulating prostate cells independent of when cells undergo EMT.

Monoclonal antibodies J591 and J415, both of which are highly specific for PSMA (61), were conjugated to the surfaces of microfluidic devices for the capture of a PSMA-expressing prostate cancer cell line, LNCaP. We have previously reported high-efficiency and high-purity capture of PCTCs from CRPC patient blood samples, as well

as LNCaP cells, with monoclonal antibody J591 (76). Here, we report relationship between the concentration of antibody in solution during functionalization and the final surface conjugated ligand density, the capture performance of monoclonal anti-PSMA antibodies for cell isolation over a range of concentrations and shear stresses within microfluidic devices, and explore competition between multiple PSMA antibodies used simultaneously.

2.3 Experimental

2.3.1 Materials

LNCaP cells, a PSMA-expressing prostate cancer cell line, were purchased from the American Type Culture Collection (ATCC; Manassass, VA). A Fusion-100 syringe pump was purchased from Chemyx (Stafford, TX). Corning CellBIND™ surface $75\,\mathrm{cm}^2$ culture flasks were purchased from ThermoFisher Scientific (Waltham, MA). Sylgard® 184 Silicone Elastomer Kit (polydimethylsiloxane, PDMS), was purchased from Dow-Corning (Midland, MI). Fetal bovine serum (FBS) was purchased from Gemini Bio-products (West Sacramento, CA). The plasma cleaner was purchased from Harrick Plasma (Ithaca, NY). The hemacytometer was purchased from Hausser Scientific (Hanshaw, PA). Dulbeccos Phosphate-Buffered Saline (PBS) solution, RPMI-1640 cell culture media, antibiotic-antimycotic solution (Penicillin-Streptomycin), and trypan blue solution were purchased from Mediatech (Manassass, VA). The Eclipse TE2000U inverted microscope was purchased from Nikon (Melville, NY). (3-Mercaptopropyl) trimethoxysilane (MPTMS), 200 proof anhydrous ethanol (EtOH), Dimethyl Sulfoxide (DMSO), Bovine Serum Albumin (BSA), Trypsin-EDTA

solution, and 1,1,2,2 tetrahydro-perfluorooctyltrichlorosilane were purchased from Sigma-Aldrich (St. Louis, MO). Harris Uni-Core™, tip diameter $0.50\,\text{mm}$, was purchased from Ted Pella (Redding, CA). (N-[γ-maleimidobutyryloxy]succinimide ester) (GMBS), NeutrAvidin Protein, EZ-Link NHS-LC-LC-Biotin, Goat Anti-Mouse IgG DyLightTM 594 secondary antibody, Reacti-Bind™ NeutrAvidin™ Coated 96-Well Black Plates, Monoclonal biotinylated murine antibodies J591 and J415 were provided by Dr. Neil Bander. A Synergy HT BioTek Plate reader was used for the immunofluorescence assays.

2.3.2 Microdevice design

Examining microfluidic devices that make use of the fluid mechanics and geometries within becomes difficult as the topologies and materials make characterization of cell adhesion difficult to quantify. Hele-Shaw flow cells, high aspect ratio devices that exhibit Stokes flow between two flat plates, provide a simple and useful platform through which to tune flow characteristics for the capture of rare cells. A Hele-Shaw flow cell facilitates analysis of defined flow characteristics, specifically shear stress, because the fluid velocity field variations in the plane of the device are often amenable to analytical solution. These devices facilitate simple visualization and mapping of shear stresses. Cell capture within the microfluidic device depends on the number of interactions a cell will have with immunocoated surfaces as well as the contributions of shear stress (76, 77). Preferable flow parameters constitute flow conditions that maximize target cell viability and capture efficiency as measured by the total number of viable captured cells as compared to those present in the original sample, and purity, which is the percent of isolated cells that match the target population. The device geometry, shown with images of captured cells, is shown in Figure 2.1 (77, 78).

This device design emulates the analytical solution for potential stagnation flow. This design maintains the linear decrease in shear stress predicted by the analytical solution along approximately half of its length. Deviations from the analytical solution result from experimentally implemented inlets, outlets, and impenetrable boundaries. Using flow through this device, each experimental run characterizes cell adhesion over a wide range of shear stresses, corresponding to those experienced within microfluidic immunocapture devices (76, 77, 79).

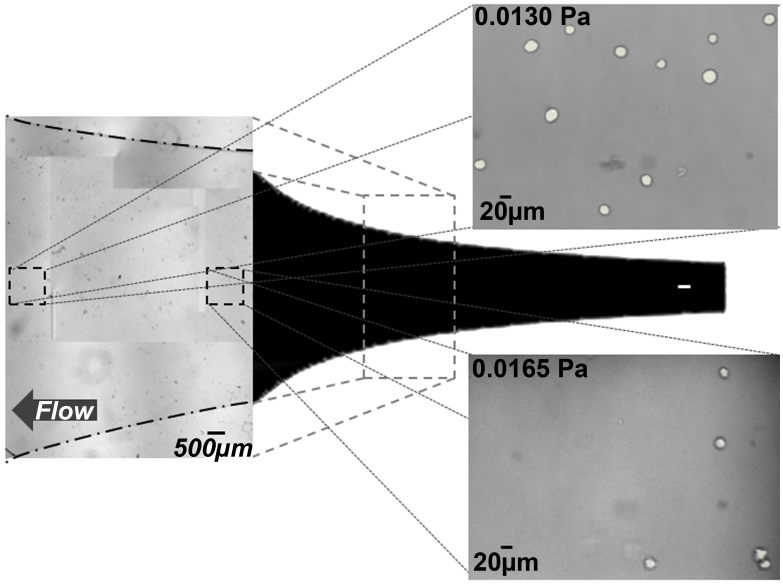

Figure 2.1: The Hele-Shaw flow cell geometry used for these experiments is defined by the streamlines of a stagnation point flow. This form generates a linear variation in shear stress along the devices centerline. Representative images of observation fields with cells immobilized on a J591-terminated surface. The locations indicated on the image correspond to local shear stresses of 0.0165 Pa and 0.0130 Pa. The listed shear stress values correspond to a device with dimensions of: depth 48 μm, length 50 mm, inlet width 5 mm; for a volumetric flow rate of 0.2 mL h^{-1}; with PBS. The shear stresses examined in these studies ranged from 0.008 Pa to 0.024 Pa.

2.3.3 Microdevice fabrication

Microfluidic device masters were created in the Cornell Nanofabrication Facility (CNF) at Cornell University using standard photolithography techniques. SU-8 Hele-Shaw device masters were fabricated by spin-coating silicon wafers with SU-8 to create a film thickness of $48\,\mu$m. The photoresist was patterned and coated with 1,1,2,2 tetrahydro-perfluorooctyltrichlorosilane, to create a non-stick coating.

This master was used to construct PDMS and glass devices. PDMS was prepared using a standard Sylgard® 184 Elastomer kit and a 5:1 ratio of the elastomer base to the curing agent and baked in a vacuum oven for a period of 8 hours at $60\,^{\circ}$C. PDMS was removed from the master, inlet and outlet holes were punched and the patterned PDMS was cleaned using an acetone and isopropyl alcohol (IPA). Glass was prepared using a standard acid (HCl) base (NaOH) wash followed by an acetone and IPA rinse. Both the glass and the PDMS were dried under a nitrogen stream. The PDMS and glass components were plasma cleaned for 40 seconds, bonded together and baked at $60\,^{\circ}$C for 4 hours.

2.3.4 Microdevice functionalization

All capture experiments described herein are conducted with monoclonal antibodies J591 and J415; both have a high binding avidity to and specificity for epitopes on the extracellular PSMA domain and minimal nonspecific binding with PSMA-negative cells (61). The glass surfaces of the Hele-Shaw microdevices were functionalized to immobilize these antibodies. Antibody functionalization of an amine-terminated surface was accomplished through a two-step process by use of incubation in 4% (v/v) MPTMS in EtOH solution for 30 minutes followed by a 20 minute incubation with a 1 mM GMBS

in EtOH solution. Next, a layer of NeutrAvidin was covalently attached to the surface by incubating the surface for 60 minutes with $25\,\mu g$ of NeutrAvidin per milliliter of PBS. Finally, the biotinylated monoclonal antibody was immobilized on the surface via the biotin-NeutrAvidin bond (61, 76, 80). Devices were stored before use in a $1\%\ (m/v)$ BSA in PBS solution for up to two hours.

2.3.5 Cell maintenance

All capture experiments were conducted with LNCaP cells, an immortalized prostate cancer cell line derived from a human prostate adenocarcinoma that is known to express PSMA (62, 71). This cell line was selected to understand the capture performance in a population completely expressing the target epitope. LNCaP cells were cultured in T75 flasks at $37\,^{\circ}C$ in a 5% CO2, humidified environment. Cells were cultured in RPMI-1640 supplemented with 10% FBS and 1% Penicillin-Streptomycin. To prepare cells for experiments, they were removed from the culture flasks and resuspended in 1 mM EDTA in $1\%\ (m/v)$ BSA in PBS for a cell suspension density of 3×10^5 LNCaP cells mL^{-1}.

2.3.6 Immunofluorescence assay

To quantify biotinylated-antibody adhesion to and saturation on the surface an immunofluorescence assay was completed. A series of solutions with different J591 mAb concentrations (0.25-$160\,\mu g\,mL^{-1}$) were prepared via serial dilution. $100\,\mu L$ of each dilution was incubated on wells of a NeutrAvidin-coated 96-well plate for 1 hour. Following incubation, all wells were washed with PBS and subsequently incubated with a $1\%\ (m/v)$ BSA in PBS solution as a blocking buffer. The blocking buffer was

removed and the wells were washed with PBS. Finally, a fluorophore-conjugated murine secondary antibody in PBS was incubated in the antibody-conjugated wells for 1 hour. After incubation, all wells were washed with PBS and read by a plate reader.

2.3.7 Capture experiments

To simulate the local shear stress experienced by cells within immunocapture microdevices, a cell suspension was flowed through the Hele-Shaw microdevices at a rate of $0.2\,\mathrm{mL\,h^{-1}}$ using a Chemyx Fusion 100 syringe pump. Subsequently, a solution of $1\%\ (m/v)$ BSA in PBS with $1\%\ (v/v)$ Trypan blue was flowed through the chamber at $0.2\,\mathrm{mL\,h^{-1}}$ for 15 minutes to wash away any non-adhered cells. Images were taken at a $20\times$ magnification under bright field at a series of predetermined observation sites along the length of the device. For the capture experiments, cell count values were collected for 14 unique shear stress regions with at least eight repetitions. For all shear stresses, the reported value corresponds to the shear stress at the wall in the center of the imaged area. The cell counts reported in each graph correspond to the number of cells imaged in a $1\,\mathrm{mm}$ region at the central axis of the Hele-Shaw flow cell associated with each reported shear stress. In comparing the performance of antibodies, a two-way ANOVA and Tukey post hoc test (α=0.05) was completed analyzing both shear stress and antibody selection as influencing factors on the number of cells isolated in each observed region.

2.4 Results

To measure the effect of antibody incubating solution concentration on bound antibody, we performed an immunofluorescence assay on J591 antibody with incubating solutions of concentration ranging from 0.25-$160\,\mu g\,mL^{-1}$. Antibody binding, as quantified by fluorescence from a functionalized secondary antibody, shown in Figure 2.2, indicates antibody saturation on the surface for an incubating solution concentration of $10\,\mu g\,mL^{-1}$ for our functionalization protocol.

We then tested whether the antibody concentrations inferred from immunofluorescence are consistent with cell capture. We captured LNCaP cells flowed through a microfluidic device with Hele-Shaw geometry and characterized the cell density as a function of local shear and antibody incubation concentration. Cell capture increased with increasing antibody concentration, as demonstrated in Figure 2.3, until the surface becomes saturated with the antibody; these results are in congruence with the immunofluorescence data. As expected, cell capture is more prominent at low shear stress.

Given that $10\,\mu g\,mL^{-1}$ antibody provides saturation-level cell capture in this system, we then investigated two antibodies and their combination to determine the optimal surface to use for PSMA+ cell capture. To measure the relative ability of different antibodies and antibody mixtures to capture PSMA-positive cells, we captured LNCaPs with two different monoclonal antibodies and a mixture of the two at constant antibody incubation concentration. Figure 2.4 shows the relative performance of biotinylated-J591, biotinylated-J415, and a 50/50 mixture of biotinylated-J591 with biotinylated-J415 on capture of LNCaPs. In all cases, $10\,\mu g\,mL^{-1}$ antibody solutions were used when functionalizing the surfaces. Similarly, the capture of LNCaP cells decreases as a function of increasing shear stress, as expected. Over the range of shear

stresses measured, captured cell density of the J415 and J415-J591 mixture were both significantly lower ($p < 0.001$) relative to J591 but not significantly different from one another.

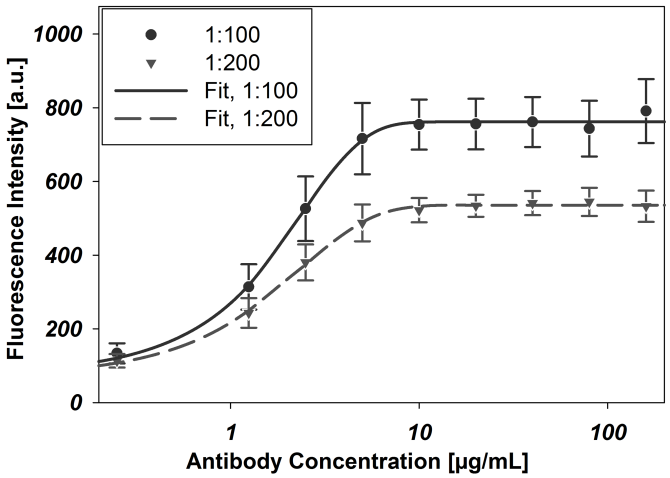

Figure 2.2: Immunofluorescence data indicate surface coverage of immobilized biotinylated-J591 on a NeutrAvidin-coated substrate. Antibody concentrations represent the concentration of antibody in the incubating solution in micrograms per milliliter. All J591 dilutions were prepared from a stock solution of concentration $2\,\mathrm{mg\,mL^{-1}}$. Unique curves indicate the dilution of the stock fluorophore-conjugated murine secondary antibody solution $2\,\mathrm{mg\,mL^{-1}}$ to PBS used to stain the surface. Error bars represent standard error of the mean, all data points are representative of six repetitions (n=6). Each curve was fit with a 4-parameter Langmuir adsorption isotherm. $\mathrm{EC50_{1:100}} = 1.5636\,\mu\mathrm{g\,mL^{-1}}$, $\mathrm{EC50_{1:200}} = 1.3848\,\mu\mathrm{g\,mL^{-1}}$.

2.5 Discussion

Although EpCAM is ubiquitous as an immunoenrichment antigen for CTCs (5, 12, 51, 52), uncertainties remain regarding the biases introduced by EpCAM capture and EMT (81). The expression of PSMA in PCa affords a new transmembrane protein that may be targeted for isolation of circulating prostate cells (64). PSMA is expressed exclusively in prostate tissues, with the exception of some neovascular endotheliae.g., renal cell carcinoma, breast cancer, gastric adenocarcinoma, and colorectal adenocarcinoma

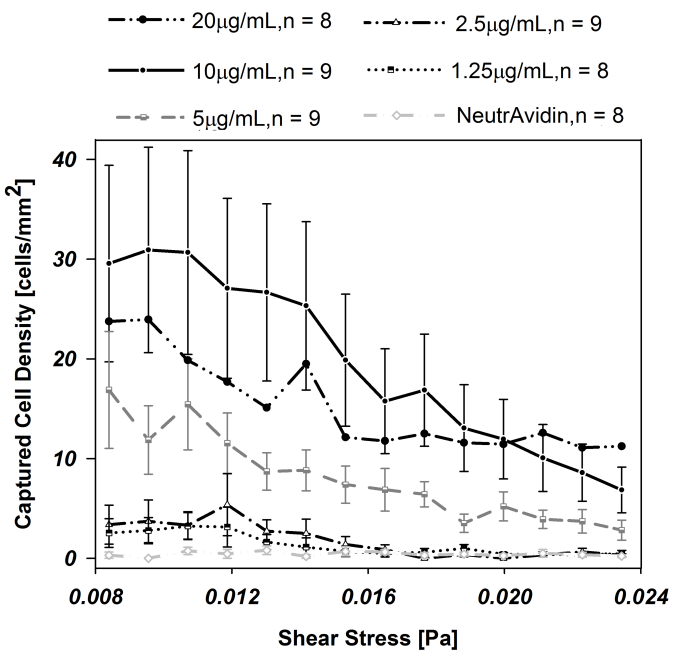

Figure 2.3: Cell adhesion to a biotinylated-J591 immunocoated substrate at varying antibody concentrations: 10 (n=9), 5 (n=9), 2.5 (n=9), and 1.25 $\mu g\,mL^{-1}$ (n=8), as a function of shear stress. Error bars represent the standard error of the mean; error bars are omitted from 20 $\mu g\,mL^{-1}$ data for clarity.

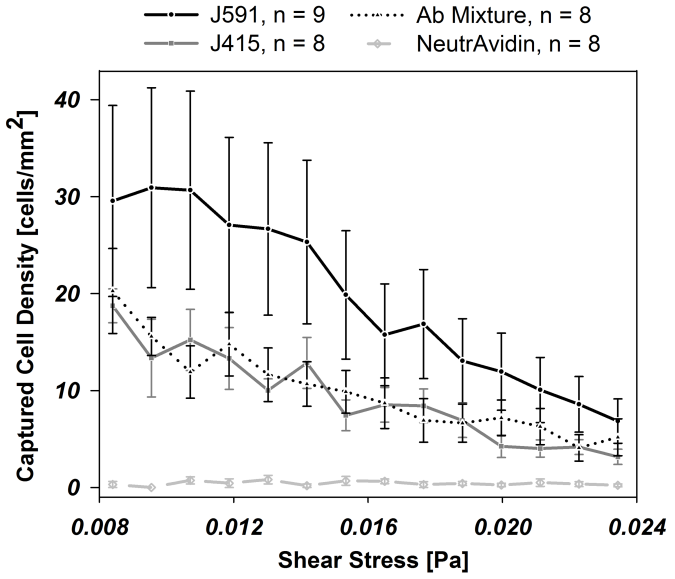

Figure 2.4: Cell adhesion to an immunocoated substrate coated with biotinylated-J591 (n=9), -J415 (n=8), a 50/50 mixture of J591/J415 (n=8), and NeutrAvidin (n=8), as a function of local shear stress, as indicated. Error bars denote the standard error of the mean.

(62, 82, 83). PSMA is also expressed at 100-1000-fold lower levels in small intestine, proximal renal tubules, salivary glands, and some astrocytes; these cell types are generally separated from the circulation by epithelial tight junctions, basement layers, or the blood-brain barrier (61, 70, 82, 84–88). These cell types are not expected in circulation.

The anti-PSMA antibodies J591 and J415 are known to target prostate cancer cells in immunotherapeutic studies and are examined in this study to quantify capture performance of PSMA-expressing cells (63, 89). PSMA exhibits three unique extracellular domains including a protease domain, an apical domain, and a C-terminal domain; all present opportunities for immunocapture (90). J591 and J415 bind to unique external epitopes on the PSMA protein (61, 69), but published data differs on their competitive nature (61, 89). As observed from Figure 2.4, the performance of J591 is superior for capture compared to J415 at all shear stresses tested ($p < 0.001$). This may be explained by differences in competition for binding at a wall with an antigen location near the cell membrane, as is the case with J415, as compared to one at the apical domain, as with J591 (61, 63, 64). Although these antibodies bind to distinct locations on the PSMA protein, there are no observed synergistic effects from a surface functionalized with a J591-J415 mixture treatment. Instead, a decreased performance as compared to the standard $10\,\mu g\,mL^{-1}$ J591 treatment resulted. This mixture performed similarly to a $5\,\mu g\,mL^{-1}$ J591 treatment. This result is consistent with steric hindrance of simultaneous access of wall-bound antibodies to apical and C-terminal domains of PSMA.

Measured saturation concentrations are in congruence with current standards for microdevice immunocapture. $10\text{-}20\,\mu g\,mL^{-1}$ is a common concentration used for surface functionalization (5, 76), and in this study, this concentration matches optimal performance in both immunofluorescence and cell capture with minimal reagent use in

this study.

The implemented microdevice facilitates simple data harvesting as a result of well-defined local shear stresses on surfaces that can be easily imaged. This platform enables the investigation of the effects of shear stress on the integrity and viability of immobilized cells; factors that must also be considered when designing microdevices for high capture efficiency and capture population purity.

The shear stress range examined can be tuned to match any microfluidic immunocapture platform of interest; thus, predictions about cell isolation can be experimentally derived before design and implementation of novel immunocapture devices (78).

2.6 Conclusions

This work characterizes PSMA+ cell capture on J591- and J415-functionalized surfaces as well as surfaces with a combination of these antibodies. J591 performed better than J415 or a combination of J591 and J415 at equal mass concentrations. Immunofluorescence characterization of surface antibody density echoed cell capture rates. Cell capture rates decrease with increasing shear stress. Anti-PSMA rare cell capture gives the potential to enrich prostate cancer circulating tumor cells without biases associated with epithelial-to-mesenchymal transitions.

Acknowledgements

The work described was partially supported by the Cornell Center on the Microenvironment & Metastasis through Award Number U54CA143876 from the National Cancer Institute, the Cornell NSF GK-12 program and the Cornell-Sloan

Fellowship (S.S.). The authors thank LJ Bonassar for use of the plate reader.

CHAPTER 3

CANCEROUS EPITHELIAL CELL LINES SHED EXTRACELLULAR VESICLES WITH A BIMODAL SIZE DISTRIBUTION THAT IS SENSITIVE TO GLUTAMINE INHIBITION

3.1 Abstract

Extracellular shed vesicles (ESVs) facilitate a unique mode of cell cell communication wherein vesicle uptake can induce a change in the recipient cell's state. Despite the intensity of ESV research, currently reported data represent bulk characterization of concentrated vesicle samples with little attention paid to heterogeneity. ESV populations likely represent diversity in mechanisms of formation, cargo, and size. To better understand ESV subpopulations and the signaling cascades implicated in their formation, we characterize ESV size distributions to identify subpopulations in normal and cancerous epithelial cells. We discovered that cancer cells exhibit bimodal ESV distributions, one small-diameter and another large-diameter population, suggesting that two mechanisms may govern ESV formation, an exosome population and a cancer-specific microvesicle population. Altered glutamine metabolism in cancer is thought to fuel cancer growth but may also support metastatic niche formation through microvesicle production. We describe the role of a glutaminase inhibitor, compound 968, in ESV production. We discovered that inhibiting glutamine metabolism significantly impairs large-diameter microvesicle production in cancer cells.

The content of this chapter, reproduced here, was submitted as a research article to *Physical Biology*. The article is titled: "**Cancerous Epithelial Cell Lines Shed Extracellular Vesicles With a Bimodal Size Distribution that is Sensitive to Glutamine Inhibition**" (20). Authors include: Steven M. Santana (SMS), Marc A. Antonyak (MAA), Richard A. Cerione (RAC), and Brian J. Kirby (BJK). Author contributions are as follows: conceived and designed experiments (SMS, BJK), performed experiments (SMS), western blot (SMS, MAA), cell transfection (MAA), analyzed the data (SMS), wrote the paper (SMS), edited the paper (SMS, BJK, MAA, RAC).

3.2 Introduction

Cells shed heterogeneous vesicular structures into their local environment and throughout the body (21–24, 26). These vesicles facilitate a unique mode of cell cell communication, akin to paracrine signaling, wherein cargo-laden packages are submitted from the originating, or parent, cell to the recipient cell. The uptake of extracellular shed vesicles (ESVs) can induce a change in the recipients' state and thus its behavior and function (2, 36, 37, 91). The changes induced by ESV uptake are as diverse as the family of messengers. ESVs, first described in the literature as exosomes in the 1970s and 1980s (92–95), have been identified and interrogated throughout the years (21, 24, 26, 31, 32, 96–98). ESVs have been described with multiple names (22) including exosomes (99, 100), microvesicles (101, 102), microparticles (103, 104), and oncosomes (33, 105), among others; the nomenclature is not currently standardized (26). The given names, to some degree, indicate provenance, function, or properties. The term *exosome* typically refers to intraendosomal vesicles released by the cell (94), whereas the term *microvesicle* typically refers to structures that bud directly from cancer cell surfaces (21, 22, 102). Tumor-released exosomes have been implicated in cancer immunity (97), whereas tumor-derived microvesicles are implicated in the development of the metastatic niche (21, 31, 91, 102, 106–109). Importantly, microvesicles are different from apoptotic bodies (110), as their contents do not merely represent a random sampling of cell constituents, but rather specifically packaged cargo (21, 110). Many assays have been executed to characterize exosome and microvesicle content (29, 111, 112), mechanisms of formation (22, 31), and biological activity (2, 99). Although ESV interrogation (22, 113–117) and clinical and commercial application (ExoQuick™; Exo-Flow™; ExoELISA™) (118–120) represent areas of intense research and activity, little has been done to characterize ESV *subpopulations*

emanating from a single cell source (102, 121). Limitations in processing techniques are presently responsible for the sparseness of subpopulation analysis to date.

Currently reported data represent bulk characterization of concentrated ESV samples with little or no attention paid to heterogeneity. ESV populations, even those that emanate from a single cell type, likely represent a diverse population with unique cargo and mechanisms of formation. To better describe ESV populations, an understanding of constituent subpopulations and the signaling cascades implicated in their formation and shedding is necessary (102). Of particular interest is the dissemination of cancer cell-derived microvesicles and their role in priming the metastatic niche. We are unaware of any thorough characterization of cancer cell-derived ESV size distributions. In this work, we characterize ESV size distributions of species sourced from model cancer cell lines to identify distinct subpopulations with a goal of informing subsequent interrogation. We compare these results, in the case of pancreatic cancer, to ESV signatures from a model normal epithelial pancreas cell line.

Among cancers, pancreatic cancer is the fourth-leading cause of cancer death in the United States (122) and the most lethal malignancy, with pancreatic ductal adenocarcinoma (PDAC) being the most common (123). The overall survival rate of pancreatic cancer is less than 5% (124). These abysmal outcomes result, in part, from a typically asymptomatic progression until late-stage cancer has developed. Clinically recommended means of early detection do not exist, even though early dissemination of tumor cells has been implicated in the low survival rates and rapid progression of pancreatic cancer (9, 19). In murine xenograft models, the interaction between cancer cells and normal pancreas cells promotes pancreatic cancer progression (38, 39); and microvesicles harvested from cancer cells interact with and change the state of stromal cells (21, 40, 41). These results indicate that, in pancreatic cancer, cancer cell-derived

microvesicles can transform normal cells and prime the tumor microenvironment.

Pancreatic cancer often results from mutations in the *RAS* family of genes, typically *KRAS* (19, 125–127). In cells, the binding of guanosine triphosphate (GTP) to KRAS results in its activation (126, 128) and ability to initiate signaling cascades that promote cell proliferation, migration, and differentiation (126, 128). Mutations that cause KRAS to be in a persistently active, GTP-bound state send excessive signals that stimulate cell growth, thus contributing to tumor formation (126, 129, 130). Recently, modification of glutamine metabolism by oncogenic *KRAS* has been identified as a primary player in maintaining tumor growth and survival (131–136). Consequently, the ability to metabolize glutamine is markedly increased as the cell relies more heavily upon anabolic processes (132, 137, 138). These alterations in cellular metabolism are thought to provide the fuel necessary not only for cancer cell growth but also for microvesicle (MV) production. Given that altered glutamine metabolism results from the ubiquitous KRAS mutations, among other causes (139, 140), in pancreatic cancer, we investigated the effect that treating model pancreatic cancer cell lines with glutaminase inhibitor, compound 968, would have on ESV production. We discovered that inhibiting glutamine metabolism blocked the ability of pancreatic cancer cell lines to generate MVs. These findings underscore the functional connections between the altered metabolic state of cancer cells and their ability to generate ESVs.

3.3 Methods

3.3.1 Cells and Culture

U87 MG (U87, HTB-14^{TM}, glioblastoma), MDAMB231 (HTB-26^{TM}, metastatic mammary gland adenocarcinoma), PANC-1 (CRL-1469^{TM}, pancreatic ductal carcinoma), BxPC-3 (CRL-1687^{TM}, pancreatic adenocarcinoma), and hTERT-HPNE (CRL-4023^{TM}, hTERT-immortalized normal pancreatic duct) model cell lines were obtained from the American Type Culture Collection (ATCC®, Manassas, Virginia). U87 cells were transfected so as to stably express epidermal growth factor receptor variant III (EGFRvIII), see Section 3.3.2, which is associated with increased proliferation in glioma cells (21, 141, 142); this cell line will subsequently be referred to as U87+EGFRvIII.

Cell Culture

MDAMB231, U87, U87+EGFRvIII, and BxPC-3 cell lines were grown in Roswell Park Memorial Institute (RPMI-1640; Lonza, Walkersville, MD) cell medium containing 10% fetal bovine serum (FBS; Gemini BioProducts, West Sacramento, CA). The PANC-1 cell line was grown in Dulbecco's Modified Eagle Medium (DMEM; Mediatech, Manassas, VA) containing 10% FBS. The hTERT-HPNE cells were grown in a medium consisting of 75% DMEM (Sigma-Aldrich, St. Louis, MO) and 25% M3^{TM}Base (Incell, San Antonio, TX) containing 5% FBS. All lines were maintained at $37\,^{\circ}$C in a humidified, 5% carbon dioxide environment. The medium in each flask was exchanged every 2-3 days and rinsed with phosphate buffered saline (PBS) according to standard sterile techniques. All cell cultures are maintained in $25\,\mathrm{cm}^2$ rectangular cell culture

flasks.

3.3.2 Generation of Stable Cell Lines

The pcDNA3 construct encoding human EGFRvIII was transfected into U87 cells using Lipofectamine (Invitrogen, Carlsbad, CA). Clones of U87 cells stably expressing EGFRvIII were selected by culturing the cells in RPMI-1640 containing 10% FBS and $1\,\mu g\,mL^{-1}$ puromycin. Once individual clones expressing EGFRvIII were obtained, the cells were then maintained in the same growth medium supplemented with $0.3\,\mu g\,mL^{-1}$ puromycin.

3.3.3 ESV Harvesting Protocol

Prior to obtaining the ESVs, nearly confluent culture flasks were rinsed with PBS and then subjected to serum-free medium culture conditions for 12 hours. The resultant conditioned media, each from approximately 2.5×10^6 serum-starved cells, was collected for analysis. Conditioned media was centrifuged in two stages, $300\times$g for 10 minutes and $12000\times$g for 20 minutes, to pellet intact cells and cell debris, respectively. $500\,\mu L$ aliquots of the supernatant were extracted for measurement.

Cell Treatment with a Glutaminase Inhibitor

A glutaminase inhibitor, compound 968 (968; EMD Millipore, Billerica, MA), was prepared by dissolving 968 in dimethyl sulfoxide (DMSO; Sigma-Aldrich, St. Louis, MO) at $30\,mM$. 36 hours prior to ESV harvesting, cells were treated with 968 at $10\,\mu M$

(143, 144); a total of $1.67\,\mu L$ of 968 in DMSO was added to $5\,mL$ of culture medium (0.03% by volume). Following the protocol described in Section 3.3.3, cells were treated with $10\,\mu M$ 968 under serum-starved conditions for 12 hours. Subsequent harvesting and centrifugation steps are identical to those previously described.

3.3.4 Immunoblot Analysis

Cultures of cells treated as indicated were rinsed with PBS and then lysed with cell lysis buffer ($25\,mM$ Tris, $100\,mM$ NaCl, 1% Triton X-100, $1\,mM$ EDTA, $1\,mM$ DTT, $1\,mM$ $NaVO_4$, $1\,mM$ β-glycerol phosphate, $1\,\mu g\,mL^{-1}$ aprotinin, $1\,\mu g\,mL^{-1}$ leupeptin). To generate ESV lysates, the partially clarified conditioned medium (medium cleared of intact cells and cell debris), see Section 3.3.3, was filtered using a Steri-Flip PVDF filter with a pore size of $0.2\,\mu m$ (Millipore Corporation, Billerica, MA). The ESVs retained by the filter were washed thoroughly with PBS and then lysed with $300\,\mu L$ cell lysis buffer. An equal number of cells from each cell line ($5e3$ cells) and a corresponding equal ratio of ESVs generated by the cell lines were resolved by sodium dodecyl sulfate polyacrylamide gel electrophoresis (SDS-PAGE) and the proteins were transferred to PVDF membranes. The membranes were blocked in 5% dry milk diluted in TBST ($20\,mM$ Tris, $135\,mM$ NaCl, and 0.02% Tween 20), and then were incubated with Flottilin-2 (Cell Signaling, Inc., Danvers, MA), RhoC (Cell Signaling, Inc.), or actin (Sigma-Aldrich) antibodies prepared in TBST. Horseradish-peroxidase conjugated secondary antibodies were used to detect the primary antibodies, followed by extensive washing with TBST and then exposure to enhanced chemiluminescence (ECL) reagent.

3.3.5 Dynamic Light Scattering

ESV preparations were characterized at 25 °C using dynamic light scattering (DLS; He-Ne laser, 633 nm; 173°backscattered light detection) on a Nano Series Zetasizer (zetasizer, Malvern Instruments, Southborough, MA). 500 µL samples were loaded into a microcuvette (ZEN0118, Malvern Instruments) for measurement. Each measurement represents 3 unique preparations with 3 runs per preparation with at least 12 unique measurements per run. All data reported represent 108 total measurements.

3.3.6 Data Analysis

All data were processed using an author-scripted MATLAB® routine. This routine employs a nonlinear least-squares regression on multiple 4-parameter skew-normal distributions to fit each data set. The *relative scattering intensity [a.u.]* of each size distribution figure represents the volume distribution, as reported by the zetasizer which converts intensity distribution data using Mie theory; the magnitude of the figures are scaled by an arbitrary factor to enable facile comparisons among data sets. The peak amplitudes correspond to the total volume represented by the associated particle size. In all figures, unless stated otherwise, error bars represent standard error of the mean for 9 samples.

3.4 Results

The purpose of these experiments is to identify and establish distinct ESV subpopulations shed from normal and cancerous epithelial cells (MDAMB231; U87,

U87+EGFRvIII; PANC-1, BxPC-3, and hTERT-HPNE, Figure 3.1) by means of dynamic light scattering (DLS). DLS determines the size distribution of particles in solution by measuring their Brownian motion over time and measures relative sample concentrations through total recorded backscattered light. As particles move, light impinging on the particle is scattered; the time-associated scattered light readings are used to generate an autocorrelation curve. From this data, a diffusion coefficient is extracted, and thus sizes can be inferred from the Stokes-Einstein relation. A hallmark feature revealed by this investigation is the characteristic bimodal distribution of ESVs, derived from three distinct types of cancer (breast, brain, and pancreatic cancer), see Figure 3.1. Across all of the cancer cell lines, the small-diameter population exhibits a peak position of 88 ± 19 nm and an α, skewness, of 3.11 ± 1.17; the large-diameter population exhibits an average peak position of 462 ± 58 nm and an α of 2.85 ± 1.18. The skewness parameters indicate that both ESV subpopulations are dominated by the presence of the relatively larger diameter vesicles. Upon comparing the normal epithelial cell line, hTERT-HPNE, large-diameter peak position (417 ± 11 nm) and magnitude to those of the cancer cell lines, there is no statistically significant difference between the large-diameter peak position of hTERT-HPNE vesicles as compared to those of cancer cells, but approximately an order-of-magnitude difference between the peak amplitudes.

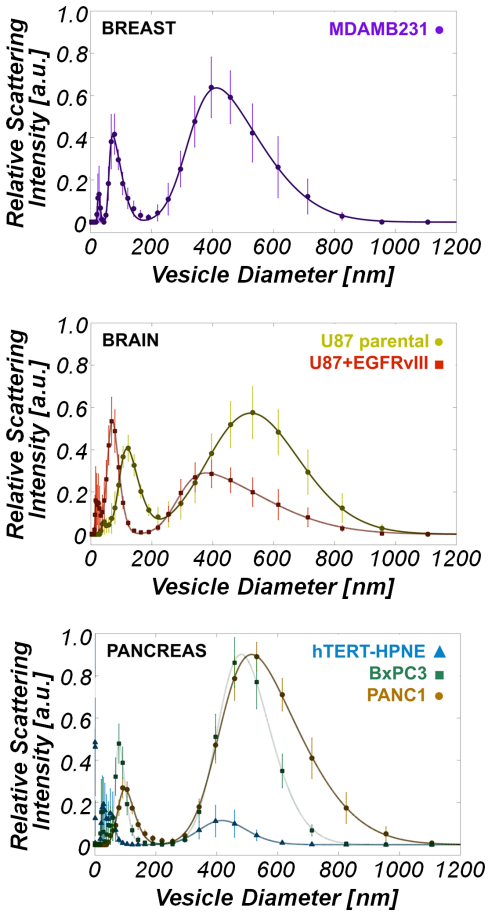

Figure 3.1: Dynamic light scattering measurements reveal a bimodal vesicle population among cancer cell types examined. *(a)* ESV size distribution in MDAMB231 cell lines. MDAMB231 peaks are located at 73 ± 1 nm and 413 ± 4 nm. *(b)* ESV size distribution in U87 and U87+EGFRvIII cell lines. U87 peaks are located at 120 ± 1 nm and 525 ± 5 nm. U87+EGFRvIII peaks are located at 70 ± 3 nm and 378 ± 2 nm. *(c)* ESV size distribution in PANC-1, BxPC-3, and hTERT-HPNE cell lines. The PANC-1 peaks are located at 98 ± 3 nm and 515 ± 3 nm. The BxPC-3 peaks are located at 80 ± 1 nm and 480 ± 2 nm. The hTERT-HPNE peaks are located at 31 ± 1 nm and 51 ± 1 nm, and 417 ± 11 nm. Of particular interest is the striking difference in ESV signatures between the normal pancreas cell line, hTERT-HPNE, and those of the two pancreatic cancer lines, BxPC-3 and PANC-1. Peaks at approximately 30 nm for the brain, breast, and BxPC-3 (pancreas) lines are an artifact of the culture medium (RPMI-1640). All deviations from the peak locations represent those values falling within the 95% confidence interval predicted by nonlinear least squares regression.

Western blots, as shown in Figure 3.2, were carried-out on the cells and the MVs that the cells shed into the medium to verify that the particles examined with DLS are

ESVs. Flotillin-2 is a protein associated with membrane transport and fusion (37, 145) and should be present in ESVs (21, 32, 32, 142). Actin, a major component of the cytoskeleton, is abundantly expressed in both whole cell lysates and ESV lysates (32, 100, 146). In the case of large-diameter ESVs that bud directly from the cell surface, it is possible that actin is essential in the maturation of budding vesicles (32). RhoC, which is involved in extracellular matrix assembly, cytoskeletal reorganization, and cell migration (147, 148), is expressed in the cytosol but is not involved in ESV formation (31). As can be seen in Figure 3.1 and 3.2, the immortalized normal epithelial cells (hTERT-HPNE) make almost undetectable levels of MVs as determined by DLS and flotillin-2 and actin staining. Furthermore, ESV preparations are devoid of cytosolic contamination as determined by the fact that RhoC is exclusively present in whole cell lysates (WCLs) and not in ESV lysates (ESVLs).

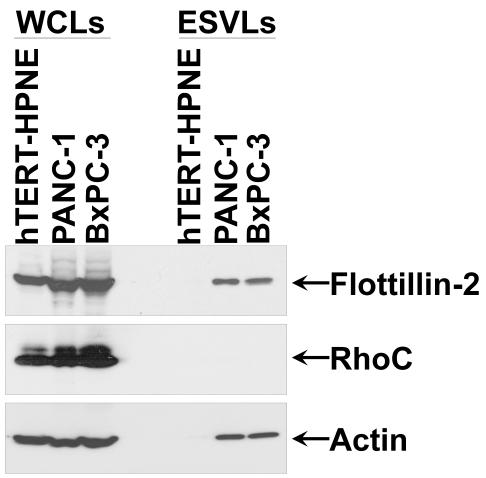

Figure 3.2: Immunoblot Assay. Serum-starved hTERT-HPNE, PANC-1, and BxPC-3 cells were lysed, and the ESVs shed into the medium by the cells were isolated and lysed as well. The whole cell lysates (WCLs) and the ESV lysates (ESVLs) were subjected to western blot analysis with antibodies against the ESV marker flotillin-2, the cytosolic-specific marker RhoC, and the loading control actin. Two blank channels separate WCLs and ESVLs.

To explore the conjecture that MVs can be related to oncogenic processes, we

asked whether glutamine metabolism, which is significantly upregulated in cancer, is important for the ability of cancer cells to generate MVs. Both cancerous epithelial cell lines, PANC-1 and BxPC-3, which rely heavily on glutamine for survival (139, 149), produced significantly more ESVs than the normal epithelial line, hTERT-HPNE. PANC-1 cells produced approximately twice as many ESVs as BxPC-3 cells. Compound 968, a glutaminase inhibitor, was added to the model pancreas lines and its impact upon ESV production was determined by DLS. We found that treating cells with compound 968 drastically altered ESV size distributions, as seen in Figure 3.3, and diminished microvesicle production, as seen in Figure 3.3 and Figure 3.4. The total calculated ESV volume for cancer cells was significantly reduced upon exposure to compound 968, but ESV volume in normal pancreas cells was not significantly affected. Relative to the non-treated cases, there was a $96.00 \pm 30.97\,\%$ reduction in total PANC-1 vesicle volume, a $97.61 \pm 28.49\,\%$ reduction in total BxPC-3 vesicle volume, and no statistically significant change in total hTERT-HPNE vesicle volume following treatment with compound 968, see Figure 3.4.

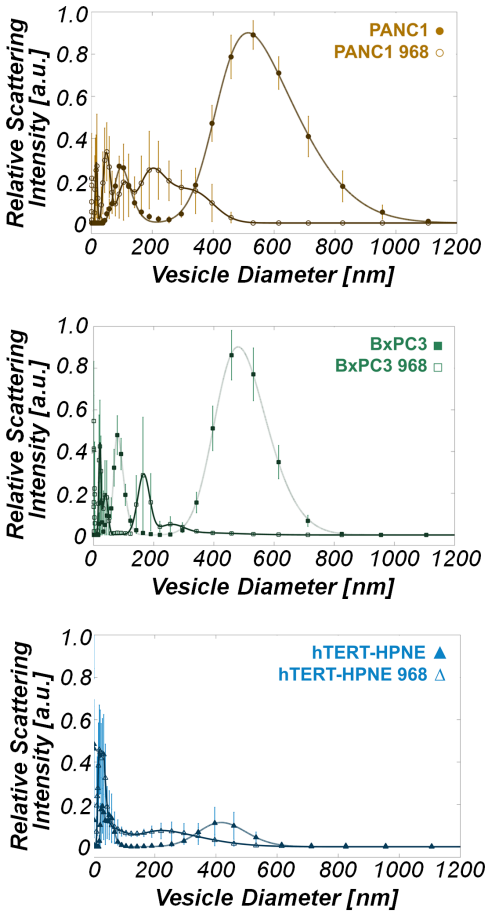

Figure 3.3: Dynamic light scattering measurements demonstrate that treatment of cancer cells with compound 968 substantially reduces large-diameter microvesicle production. *(a)* ESV size distribution in untreated PANC-1 and 968-treated PANC-1 cells. *(b)* ESV size distribution in BxPC-3 and 968-treated BxPC-3 cells. *(c)* ESV size distribution in hTERT-HPNE and 968-treated hTERT-HPNE cells. All filled markers indicate cells that have not been treated with compound 968; all outlined markers represent 968-treated cells.

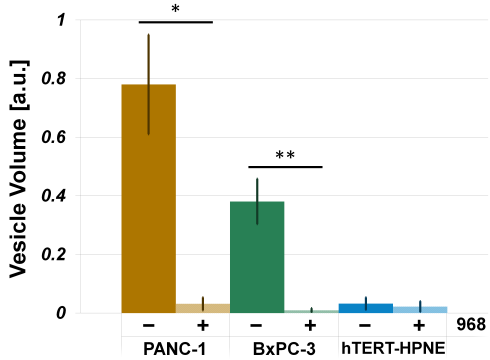

Figure 3.4: Total vesicle volume analysis demonstrates that treatment of cancer cells with compound 968 dramatically reduces vesicle production in cancer cells (PANC-1, $^{*}p = 0.0006$; BxPC-3, $^{**}p = 0.0002$) and has no statistically significant effect on vesicle production in normal epithelial cells (hTERT-HPNE, $p = 0.7$).

3.5 Discussion

We used dynamic light scattering to identify distinct cancer cell-derived ESV subpopulations. DLS has the benefit of extracting particle size distributions in a repeatable fashion and is an established, effective tool for characterizing particle sizes, including exosome populations in blood (27, 114, 121). Compared with other measurement approaches, DLS measures ESVs without requiring sample pelleting or dehydration, which could damage ESVs and alter their geometric parameters (145, 150), but does not directly report absolute particle concentration, number, or volume (116). A relative measure of total ESV volume can be calculated by integrating the product of volume percent backscattered light and ESV volume. This calculated total volume is proportional to the total vesicle volume (cargo) that could be delivered to recipient cells. Changes in total vesicle volume resulting from cell treatment or modification, such as exposure to compound 968, provides insight into changes in total ESV production resulting from treatment.

We have demonstrated the presence of two distinct subpopulations within cancer cell-derived vesicles. As suggested in other reports (21, 24, 30, 112, 116), vesicles shed by cancer cells exhibit a size range from approximately 20 nm to over 1 µm; our findings, for breast, brain, and pancreas cells, as shown in Figure 3.1, are consistent with this reported range. For each cancer cell line examined herein, the peak locations, skewness, and areas of the bimodal ESV distributions were quantified by fitting multiple 4-parameter skew-normal distributions by nonlinear least squares regression. Given the narrow range of peak positions and magnitudes for each cancer cell-derived ESV subpopulation, these data suggest that the processes governing ESV production for both small- and large-diameter vesicles may be tightly regulated and conserved across cancer types (102, 145). Despite similarity in ESV size distributions among cancer types, PANC-1 cells, which express oncogenic KRAS, produce substantially more ESVs than do BxPC-3 cells, which express wild-type KRAS (151). The presence of small- and large-diameter populations in cancerous epithelial cell lines suggests that two unique mechanisms may govern the biogenesis of each unique subpopulation (22, 102). It is possible, although yet to be determined, that the small-diameter population is representative of a normal cell exosome signature and that the large-diameter vesicles represent an aberrant, cancer-related microvesicle signature. Evidence in a small cohort of stomach and liver cancer patients (152, 153) further bolsters this claim.

We determined that in the cell lines considered large-diameter ESVs (microvesicles) are a cancer-specific signature associated with dysregulated glutamine metabolism. Cancer activates, upregulates, modifies, or creates specific signaling cascades that are dysregulated versions of host pathways not expressed under normal conditions (31, 135, 154, 155). Given the role of glutamine metabolism in pancreatic cancer (126, 130–132, 139, 140), we explored the impact of a glutaminase inhibitor, compound

968, on microvesicle production. Compound 968 has been shown to inhibit cancer growth but has no impact on the proliferation of normal cells (143, 156, 157). We found that the results of treating cells with this glutaminase inhibitor included a preferential reduction in the large-diameter vesicle population, see Figure 3.3, and a drastic reduction in total vesicle production, as shown in Figure 3.3 and Figure 3.4. This outcome is consistent with the hypothesis that large-diameter ESVs (microvesicles) are cancer-specific, as the introduction of a glutaminase inhibitor significantly disrupted their production in cancer cells but only had a limited effect on normal epithelial cells, see Figure 3.3. These data also suggest that treating cancer cells with glutaminase inhibitors may serve as a means not only to preferentially starve, and perhaps eliminate, cancer cells (143, 158), but also as a way to restrict their MV production, which could reduce their ability to prepare the metastatic niche (2, 27, 28, 107). More work is necessary to appropriately interrogate and describe the role of glutaminase inhibitors in ESV production in cancer.

3.6 Conclusion

Understanding the mechanisms of ESV generation, as well as their cargo and properties, is essential. This is particularly crucial, as ESVs putatively induce changes of state in recipient cells and prime local environments for primary and metastatic tumor establishment and growth. As metastases are responsible for 90% of cancer-related death (1, 2), unlocking the processes by which ESVs are prepared provides insight into cancer treatment and inhibition of its progression. We discovered that inhibition of glutamine metabolism in model cancer cell lines significantly impairs large-diameter microvesicle production. This result suggests that vesicle formation in cancer cells can be reduced by applying a metabolic inhibitor and indicates that the large-diameter

population may be representative of cancer cell-derived microvesicles. We have also characterized the size distributions and total relative volumes of ESVs from multiple model cell lines of primary tumor and metastatic origin, as well as a normal epithelial cell line. We discovered that each cancer cell population exhibits a bimodal distribution of vesicles, including one small population of particles with diameters less than approximately $200\,\text{nm}$ and another large population bearing a diameter range from approximately $200\,\text{nm}$ to $1.10\,\mu\text{m}$. The presence of a significant large-diameter ESV population appears only in cancer cells and not in normal epithelial cells. This feature of ESV subpopulations bolsters the argument that there may be two mechanisms governing ESV formation, a small-diameter, exosome, population and a large-diameter, cancer-specific, microvesicle population. Further investigations are required to definitively establish the specific signaling cascades that govern ESV formation processes, as this could elucidate both mechanisms of vesicle formation and vesicle roles in priming the metastatic niche.

Acknowledgements

This work was supported by the National Cancer Institutes under Award Number U54CA143876, the National Science Foundation GK-12 Program under Award Number 0841291, and the Alfred P. Sloan Foundation. hTERT-HPNE cells were provided by National Institutes of Health Physical Sciences in Oncology Network Bioresource Core Facility.

CHAPTER 4

MICROFLUIDIC ISOLATION OF CANCER-CELL-DERIVED MICROVESICLES FROM HETERGENEOUS EXTRACELLULAR SHED VESICLE POPULATIONS

4.1 Abstract

Extracellular shed vesicles, including exosomes and microvesicles, are disseminated throughout the body and represent an important conduit of cell communication. Cancer-cell-derived microvesicles have potential as a cancer biomarker as they help shape the tumor microenvironment to promote the growth of the primary tumor and prime the metastatic niche. It is likely that, in cancer cell cultures, the two constituent extracellular shed vesicle subpopulations, observed in dynamic light scattering, represent an exosome population and a cancer-cell-specific microvesicle population and that ESV size provides information about provenance and cargo. We have designed and implemented a novel microfluidic technology that separates microvesicles, as a function of diameter, from heterogeneous populations of cancer-cell-derived extracellular shed vesicles. We measured cargo carried by the microvesicle subpopulation processed through this microfluidic platform. Such analyses could enable future investigations to more accurately and reliably determine provenance, functional activity, and mechanisms of transformation in cancer.

The content of this chapter is in preparation for submission. Authors include: Steven M. Santana (SMS), Marc A. Antonyak (MAA), Richard A. Cerione (RAC), and Brian J. Kirby (BJK). Author contributions are as follows: conceived and designed experiments (SMS, BJK), designed microfluidic device (SMS), performed experiments (SMS, MAA), analyzed the data (SMS), wrote the paper (SMS), edited the paper (SMS, BJK, MAA, RAC).

4.2 Introduction

Extracellular shed vesicles (ESVs), including *exosomes* and cancer-cell-derived *microvesicles*, are disseminated throughout the body (21–24, 26). We use the term *exosome* to refer to ESVs contained within multivesicular bodies (MVBs) that are trafficked to the cell surface and released via fusion of MVBs with the cell membrane. Exosomes are thought to be generated by both normal and cancerous cells (2, 94). We use the term *microvesicle* to refer to ESVs that bud from cancer cell surfaces (21, 22, 102). ESVs represent an important conduit of cell communication (2, 36, 37) and have potential as a disease state biomarker (28, 102, 153, 159, 160). ESVs contain membrane-associated, cytosolic, and nuclear molecules including specifically packaged signaling proteins, enzymes, miRNAs, and RNA transcripts (22, 27–35). Recipient cells, upon ESV uptake, can experience a change in their behavior and function (2, 36, 37) due to cargoes in the ESVs. ESVs play a role in many systems, including immune responses (37, 161, 162), reproduction (163, 164), virus proliferation (99, 145, 150), and cancer progression (2, 24, 102). Cancer-cell-derived ESVs represent a heterogenous population that exhibits a large range of sizes with unique subpopulations (20, 21, 24, 30, 112, 116). We have recently demonstrated that cancer-cell-derived ESVs exhibit a bimodal size distribution (20). It is likely that the two constituent cancer-cell-derived ESV subpopulations in this size distribution represent an exosome population and a cancer-cell-specific microvesicle population (20) and that size correlates with biological properties of interest (102, 145). Microvesicles are ubiquitous in populations shed by cancer cells and decorate the surface of these cells (20, 21).

ESV characterization is difficult because ESVs are small and exist in a complex biological milieu. The ability to discern chemical, biological, or physical differences among ESV subpopulations emanating from the same cell population is extremely

challenging. Current microvesicle harvesting approaches concentrate ESVs by means of ultracentrifugation (112, 115, 165), filtration (21, 100, 114, 166), and immunoaffinity (25, 146, 167), or some combination thereof. Although centrifugation and immunoaffinity approaches enable measurements reflecting averaged properties of heterogeneous ESV populations, they neither enable subpopulation cargo analysis nor efficiently isolate an intact ESV subpopulation for use in a biological assay. Centrifugation and filtration can concentrate ESVs within a sample, but centrifugation does not separate subpopulations. Filtration can isolate a targeted size population, but, to date, the recovery efficiency and purity have not been quantified. Furthermore, pressure drops across filters may damage the isolated ESV subpopulation.

To address these limitions, we have designed and implemented a novel microfluidic technology that separates microvesicles, as a function of diameter, from heterogeneous populations of cancer-cell-derived extracellular shed vesicles by using the principles of deterministic lateral displacement (DLD) (168, 169). Microfluidic devices can be designed to control particle trajectories as a function of their properties (6, 42, 169–175). Microfluidic obstacle arrays for controlling particle trajectories have broad utility in medicine and biology (168, 169, 176, 177). These technologies tend to separate particles with diameter between approximately 1–10 μm (76, 178); as such, convection dominates transport within these systems, given fluid velocities, target particle diameters, and obstacle array dimensions. Unique considerations must be taken into account when designing devices to isolate microvesicles from extracellular shed vesicles which have diameters between approximately 10 nm–1 μm, as diffusional transport always plays a significant role for small-diameter species (169, 172).

4.3 Materials and Methods

4.3.1 Device Fabrication

The device geometry was drawn using L-Edit® (Tanner Research, Inc., Monrovia, CA). A chrome-plated quartz mask was fabricated using a DWL2000 (Heidelberg Instruments Mikrotechnik, GmbH, Heidelberg, Germany) and stripped of excess resist and chrome on a Hamatech-Steag Mask Processor (Süss MicroTec, Sunnyvale, CA). 100-mm silicon wafers were aggressively descummed with an oxygen plasma, dry-stripping process using an Aura 1000 Resist Strip (Gasonic Instruments, Inc., Calgary, Alberta). All wafers were primed under vacuum with hexamethyldisilazane (HMDS) using a YES-LP III Vapor Prime Oven (Yield Engineering Systems, Inc., Livermore, CA). This process yields an HMDS monolayer that promotes adhesion of the photoresist polymer to the wafer. To deposit the photoresist, Megaposit® SPR®220-3.0 (Shipley Company, L.L.C., Marlborough, MA), 3 mL were deposited onto the primed wafer. Following deposition, the wafer was spun at $4000\,\mathrm{r}\cdot\mathrm{min}^{-1}$ for 30 seconds to yield an approximately 3-μm layer. To cure the photoresist, wafers were soft baked at 115 °C for 90 seconds. Wafers were patterned with the mask bearing the image of the device geometry on a High Resolution Mask Aligner (ABM, Inc., Silicon Valley, CA) by exposing for 6 seconds with 365 nm light at $11.2\,\mathrm{mW\,cm}^{-2}$. Patterned wafers were subsequently hard baked at 115 °C for 90 seconds. Wafers were developed for 120 seconds in AZ® 726 MIF Developer (AZ Electronic Materials USA, Corp., Somerville, NJ) on a Hamatech-Steag Wafer Processor (Süss MicroTec, Sunnyvale, CA). To etch channels, wafers were Bosch-etched on a Unaxis 770 Deep Silicon Etcher (Oerlikon, Pfäffikon, Switzerland) to a depth of approximately 100 μm, as measured on a NewView™ 7300 3D Optical Surface Profilometer (Zygo Corp., Middlefield, CT). To remove the remaining

photoresist, wafers were piranha cleaned using a Hamatech Hot Piranha (Süss MicroTec, Sunnyvale, CA) and dry-stripped using an Aura 1000 Resist Strip, as previously described. For storage, prior to use, wafers were coated with uncured SPR®220-3.0 and diced on a K&S® 7100 Dicing Saw (Kulicke & Soffa Industries, Inc., Fort Washington, PA). All stages of device fabrication were completed in the Cornell Nanoscale Science and Facility (CNF).

4.3.2 Device Construction

Polydimethylsiloxane (PDMS) gaskets were made in a 5:1 elastomer base-curing agent ratio, using a Sylgard® 184 silicone elastomer kit (Dow Corning®, Midland, MI). PDMS gaskets were cured at $60\,^{\circ}\mathrm{C}$ for 4 hours. After curing, gaskets were cut to size and cleaned with acetone, isopropanol, and deionized water; gaskets were dried with compressed nitrogen gas. Devices were stripped of photoresist as described in Section 4.3.1. Immediately following stripping, PDMS gaskets and cleaned devices were primed for bonding in a Glen 1000 Plasma Strip (Yield Engineering Systems, Inc., Livermore, CA) with an oxygen plasma at $0.4\,\mathrm{torr}$ at $100\,\mathrm{W}$ for 180 seconds. Silicon devices and PDMS gaskets were manually aligned and bonded and subsequently baked at $60\,^{\circ}\mathrm{C}$ for 1 hour to secure the bond between the gasket and the device. Device inlets and outlets were fitted with 50-µm inner diameter Tygon® tubes (Saint-Gobain Performance Plastics, Corp., Akron, OH); devices were manually primed with ethanol.

4.3.3 Surface Modification

Devices were functionalized with 5000-Da silanated polyethylene glycol (silanated-PEG, Nanocs, Inc., New York, NY) by incubating the sealed device with $1\,\mathrm{mg\,mL^{-1}}$ silanated-PEG in $95\,\%$ ethanol, $5\,\%$ deionized water $(vol./vol.)$ for 120 minutes. To remove the PEG solution, devices were rinsed with ethanol, purged with deionized water, and then with $3\%(m/v)$ bovine serum albumin (BSA) in phosphate buffered saline (PBS) (3% BSA buffer). Devices were stored in 3% BSA buffer, at room temperature, for up to 4 hours prior to use.

4.3.4 Cell Culture

The BxPC-3 (CRL-1687™, pancreatic adenocarcinoma) cell line was obtained from the American Type Culture Collection (ATCC®, Manassas, Virginia) and cultured in Roswell Park Memorial Institute (RPMI-1640; Lonza, Walkersville, MD) cell medium containing 10% fetal bovine serum (FBS; Gemini BioProducts, West Sacramento, CA). Cells were cultured under standard conditions ($37\,^{\circ}$C, humidified, 5% carbon dioxide environment). The culture medium was exchanged regularly according to standard sterile techniques. The cells were maintained in 25-cm^2 rectangular cell culture flasks and 150-mm cell culture dishes.

4.3.5 Sample Preparation

Fluorescent polystryene microspheres, ($1\,\%$ $(vol./vol.)$; Bangs Laboratories, Inc., Fishers, IN), of diameters $51\,\mathrm{nm}$, $190\,\mathrm{nm}$, and $2.01\,\mu\mathrm{m}$, were used to characterize microdevice performance. These beads were suspended in 3% BSA buffer by mixing

10, 30, and $50\,\mu$L of stock bead solution, respectively, in 1 mL of the 3% BSA buffer solution.

ESVs were harvested from BxPC-3 cells by collecting the conditioned medium from 30×10^6 cells subjected to a 12-hour serum starvation. Following medium collection, intact cells and cell debris were removed by centrifugation at $300\times$g for 10 minutes and $12\,000\times$g for 20 minutes. Partially clarified conditioned medium was collected for subsequent processing. To analyze microvesicle content, the supernatant sample was filtered through a $0.22\,\mu$m Steriflip® filter (EMD Millipore, Billerica, MA) and rinsed with 5 mL of PBS. Microvesicles retained on the filter surface were then lysed with 2 mL of cell lysis buffer (25 mM Tris, 100 mM NaCl, 1% Triton X-100, 1 mM EDTA, 1 mM DTT, 1 mM $NaVO_4$, 1 mM β-glycerol phosphate, $1\,\mu$g mL^{-1} aprotinin, $1\,\mu$g mL^{-1} leupeptin). $200\,\mu$L supernatant samples were extracted for each ELISA measurement. For the conditioned media controls, 200-µL of supernatant was collected. For microdevice processing, 170-µL conditioned media supernatant samples were added to $30\,\mu$L of fluorescent bead samples, for flow verification purposes, and coprocessed with a 3% BSA buffer sheath flow. Following microdevice processing, $200\,\mu$L of device outputs δ, undeflected (heterogeneous ESV) output, and ϵ, deflected (microvesicle) output, were analyzed (see Figure 4.1 for output locations).

4.3.6 Experimental Visualization and Setup

All experiments were conducted on the stage of a Nikon® LVUDM100 upright microscope (Nikon Instruments, Inc., Melville, NY). An X-cite® fluorescence illumination source (Lumen Dynamics Group, Inc., Mississauga, ON) excited and visualized fluorescent nano- and microspheres through a fluorescein isothiocyanate (FITC), Texas Red/Cy3.5, and 4',6-diamidino-2-phenylindole (DAPI) cube (Chroma

Technology Corp., Bellows Falls, VT). All images were collected with Q-Capture Pro 7™ (Quantitative Imaging, Corp., Surrey, BC) and an EXi Blue™ fluorescence microscopy camera (Quantitative Imaging). All image intensity datasets were extracted from a 500-frame, 60-fps averaged camera feed with ImageJ.

The buffer solution and prepared samples were delivered through the device by syringe pumps (Chemyx, Inc., Stafford, TX) at a rate of $3.74\,\mathrm{mL\,h^{-1}}$ and $0.15\,\mathrm{mL\,h^{-1}}$, respectively. The effluent of each outlet was collected in 1.5 mL tubes (Eppendorf, AG, Hamburg, Germany).

4.3.7 ELISA

Vascular endothelial growth factor (VEGF) content was measured at the output ports of interest with the Human VEGF Quantikine ELISA Kit (R&D Systems, Inc., Minneapolis, MN) according to the manufacturer's instructions. Concentration readings were scaled and adjusted to account for diluents (3% BSA, lysis buffer, PBS, and serum-free RPMI).

4.3.8 Data analysis

All statistics were extracted using Matlab®. Reported errors represent standard error of the mean for six measurements, unless noted otherwise. To eliminate background noise from the output readings, the integral of total pixel intensity for all regions of interest was used to adjust the intensity reading of each channel. To calculate output channel purity, the product of the output channel composition and the volume integral of ESVs produced by BxPC-3 cells was calculated.

4.4 Results and Discussion

A microfluidic device, Figure 4.1, was designed to separate microvesicles from samples containing heterogeneous extracellular shed vesicle populations by use of deterministic lateral displacement (169). The threshold diameter, *i.e.* the diameter above which particles experience deterministic lateral displacement resulting from interactions with the obstacle array, is $250\,\mu$m, as seen in Figure 4.2a. The threshold diameter is dictated by the array properties, see Figure 4.1b. This threshold diameter is designed to lie in the natural gap existing between the two cancer-cell-derived ESVs subpopulations shed by BxPC-3 cells (20). The array geometry could be tuned to efficiently separate species with unique threshold diameters (42, 171). In this system, the Peclet number (Pe), that is, the ratio of convective to diffusional transport rates, is significantly greater than unity ($Pe = \mathcal{O}(10^7 - 10^9)$) and is calculated as $Pe = \frac{\Lambda\langle U_{\text{flow}}\rangle}{D}$, where Λ is the center-to-center obstacle spacing in the direction of flow (see Figure 4.1), $\langle U_{\text{flow}}\rangle$ is the average fluid velocity, and D is the particle diffusivity dictated by the Stokes-Einstein equation ($D \propto \frac{1}{d_{\text{particle}}}$). As such, flow-associated transport is dominated by convection. In the direction orthogonal to the mean direction of flow, transport is mediated by deterministic lateral displacement (DLD) (168, 169) and by diffusion, to varying degrees, as a function of the particle diameter (d_{particle}). The relative transport contributions of these phenomenon can be directly compared in the ratio of the characteristic diffusional transport length ($l_{\text{diffusion}}$) and the characteristic DLD transport length (l_{DLD}), that is $\frac{l_{\text{diffusion}}}{l_{\text{DLD}}} = \sqrt{\frac{D}{U_{\text{DLD}}^2\tilde{t}}}$, where the characteristic time scale, $\tilde{t}$, is derived from microfluidic array properties and the flow rate $\tilde{t} = \frac{\Lambda}{\langle U_{\text{fluid}}\rangle}$, and U_{DLD} is the transverse velocity of the particles resulting from deterministic lateral displacement. Figure 4.2b shows the value of this transport ratio as a function of ESV diameter. In the case of small-diameter ESVs (*i.e.* exosomes), which are on the order of 10–$100\,$nm, diffusional transport plays

a significant role. As such, diffusion may limit a particle's ability to enter a collision-mode trajectory, as mediated by DLD, and decrease the device's separation efficiency (172).

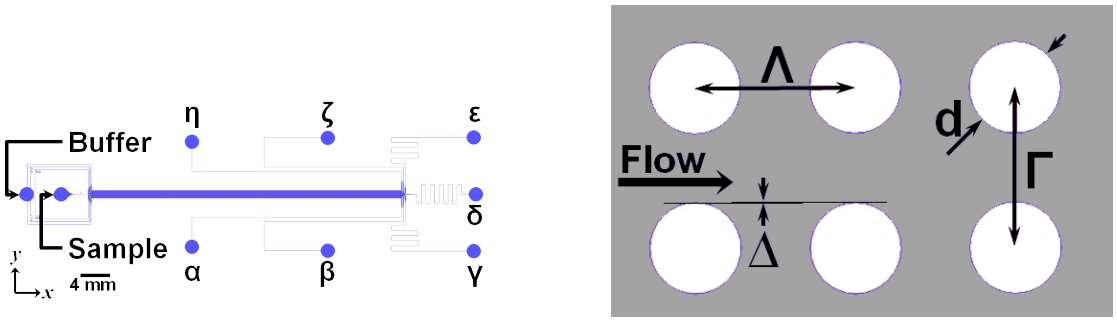

(a) (b)

Figure 4.1: Microfluidic Microvesicle Separation Device Design. *(a) Device Schematic.* Note that the microvesicle sample is centered on the input and is surrounded by a sheath flow. Particles (microspheres and ESVs) experience a symmetric and effectively infinite flow field. The volumetric flow rate of each input channel, buffer and sample inputs, has been matched to ensure uniform input velocity. The mean flow is in the x-direction; the mean fluid flow in the y-direction is zero. In this system, output ϵ contains the displaced microvesicle population and output δ contains the heterogeneous ESV population. *(b) Post Array Design.* The geometric parameters are designed to yield a threshold diameter of 250 nm. The center-to-center spacing are indicated by Λ and Γ. The obstacle diameter is indicated by d. The offset is indicated by Δ. the shoulder-to-shoulder gap is $6\,\mu$m and the offset angle is $0.16°$.

The post array and device geometry were designed in an incremental process. Approximate particle trajectories in this system were predicted by means of a ballistic model (171); this approach predicts trajectories for dilute particles treated as Lagrangian tracers experiencing inelastic obstacle collisions (171). The ballistic model provides a baseline obstacle array geometry from which subsequent designs are based. Subsequently, a finite element modeling (FEM) approach (171) was used to predict the threshold diameter and resultant particle trajectories and displacements. Informed by the FEM data, iterative changes were made to the array's geometric parameters, accounting for device length, pressure drops, and diffusional transport, until the target threshold diameter, 250 nm, and total displacement across the device

length, $\mathcal{O}(100\,\mu\text{m})$, were achieved. The total displacement is designed to yield a spatial separation that overcomes small-diameter particles' diffusion across the device length. The displacements resulting from the final array, as shown in Figure 4.1b, are shown in Figure 4.2a. On-device microvesicle separation performance was evaluated

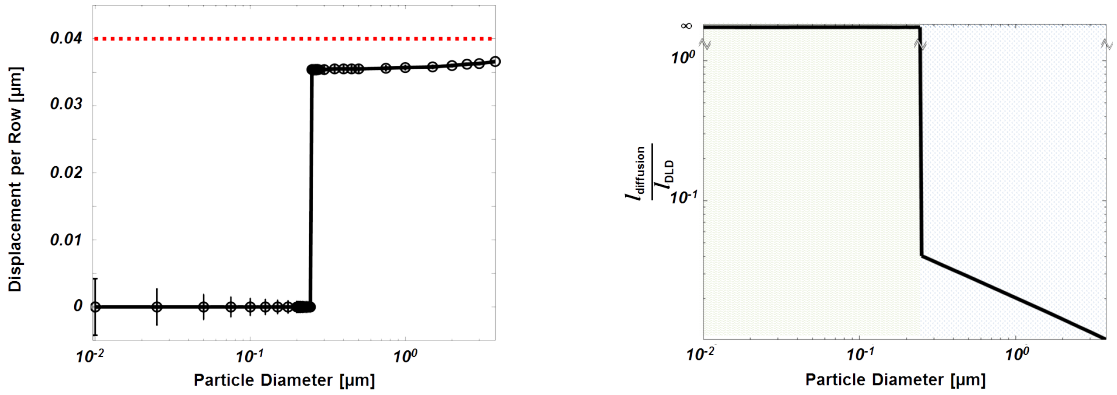

(a) (b)

Figure 4.2: Device Performance and Transport. *(a) Calculated Displacement.* The total calculated displacement per obstacle as a function of ESV diameter was determined by FEM (COMSOL). The markers represent calculated displacement accounting for particle–obstacle interactions; the vertical bars represent the maximum possible displacement resulting from diffusional transport over the timescale between obstacle interactions. This diffusional transport is a function of particle diameter ($\propto Re_{\text{flow}} \frac{\Gamma}{d_{\text{particle}}}$, where Γ is the center-to-center spacing in the direction transverse to flow, and Re_{flow} is the Reynolds number of the flow). The curvature in the displacement curve for ESV diameters above the threshold diameter is a consequence of diameter-dependent particle migration resulting from obstacle interactions. The dashed line indicates the maximum theoretical displacement per row. *(b) Transport Length Ratio.* The ratio of the characteristic diffusional transport length to the characteristic deterministic lateral displacement (DLD) transport length as a function of particle diameter demonstrates that multiple transport phenomena must be considered in a separation device. For the device described in this work, small-diameter ESVs (below the threshold diameter) move laterally by diffusion (indicated by field of "$\sim$"). Large-diameter ESVs (microvesicles with diameters above the threshold diameter) move laterally by DLD-dominated transport (indicated by field of "$>$"), and the role played by diffusion decreases with particle size.

by processing three sets of fluorescent microspheres whose diameters represent ESV diameters of interest, one whose diameter is below the threshold diameter ($51\,\text{nm}$),

one whose diameter is less than but near the threshold diameter (190 nm), and one above the threshold diameter (2.01 µm). As shown in Figure 4.3, microspheres with diameters less than the 250-nm threshold diameter were negligibly displaced whereas microspheres with diameters above the threshold diameter were displaced, by means of deterministic lateral displacement, into the adjacent output (output ϵ). For the 190 nm-diameter population, the population with a diameter near the threshold, there is some degree of device-mediated displacement in excess of diffusion, as indicated by the composition of this population in output ϵ. In comparing output ϵ to output δ, there is a significant concentration of microvesicle-sized species in output ϵ, in accordance with the device design. The microvesicle-concentrated output, output ϵ, is $98.5 \pm 31.6\%$ pure, by volume, with a recovery efficiency of $39.3 \pm 12.4\%$.

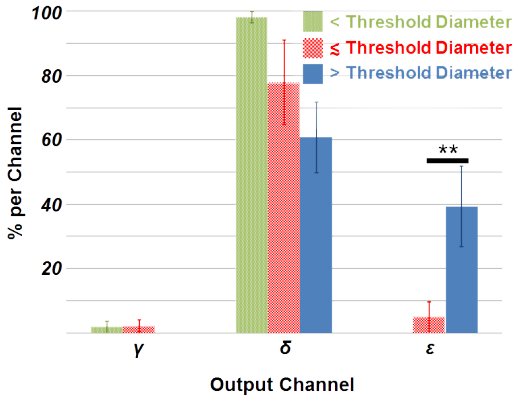

Figure 4.3: In polystyrene bead separation experiments, the microfluidic obstacle array preferentially deflects large-diameter particles in the target output (ϵ). Particles with diameters below the threshold diameter demonstrate minimal deflection from the input stream across the length of the device. Particles with diameters near the threshold diameter indicate a minimal degree of device-mediated deflection into output ϵ. There is a statistically significant difference between the composition of large- and intermediate-diameter particles in output ϵ ($p < 0.05$). *Note*: "$<$ Threshold Diameter" indicates 51 nm particles;"$\lesssim$ Threshold Diameter" indicates 190 nm particles; "$>$ Threshold Diameter" indicates 2.01 µm particles.

Following validation of this novel microfluidic platform, by means of polystyrene nano- and microsphere separation, we processed ESVs harvested from BxPC-3 cells

through the microfluidic device. As ESVs are not readily visualized during separation experiments, given their size and the similarity of their optical properties to those of the buffer solution, ESV-containing conditioned media samples were supplemented with fluorescent microspheres to verify flow separation. The fidelity of this approach for microvesicle chemical analysis was determined by quantifying the amount of VEGF present within the effluent of output δ, the heterogeneous-ESV containing output, and output ϵ, the microvesicle-containing output. We selected VEGF detection as an exemplary chemical readout, as VEGF *(a)* stimulates angiogenesis, *(b)* is found in cancer-cell-derived ESVs (22, 28, 179), and *(c)* promotes metastasis (180–182). As

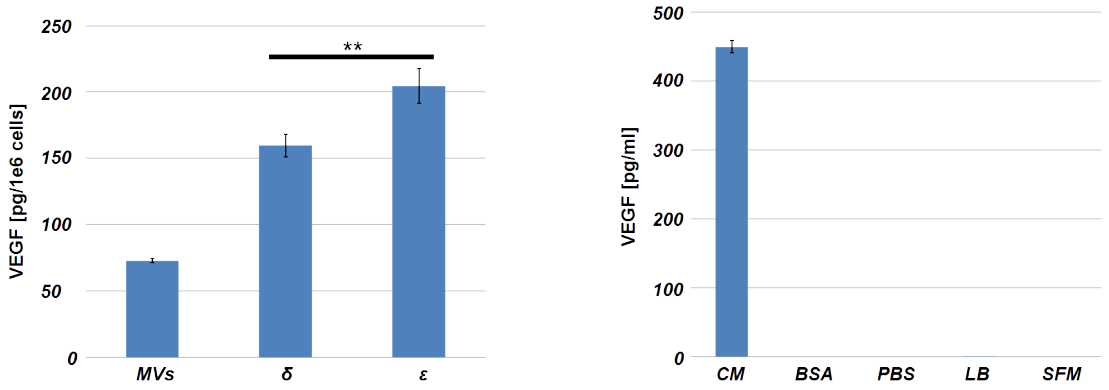

(a) (b)

Figure 4.4: *(a) VEGF Readings.* An ELISA assay was used to measure the total VEGF content in concentrated microvesicles harvested from 35 mL of BxPC-3 conditioned medium, and from 200 µL samples collected from output δ and ϵ of the microfluidic device, all measurements are scaled by total cell numbers and volume harvested, and are adjusted by the volume of diluent added. These measurements show that processing conditioned medium directly in the microdevice affords sufficient sample for immunodetection. The statistically significant difference ($p < 0.05$) in results between the VEGF content of the unique outputs likely results from the preferential concentration of microvesicles in output ϵ as compared to δ. *(b) Controls.* VEGF measurements were conducted on the following controls: unlysed conditioned medium (UCM), BSA, PBS, lysis buffer (LB), and serum-free medium (SFM). BSA, PBS, LB, and SFM are diluents in various measurements, the controls demonstrate that none but soluble VEGF in conditioned medium contribute additional VEGF to output readings. *Note*: $n = 2$ for all controls, except the conditioned medium.

shown in Figure 4.4, output ϵ has higher VEGF content than output δ; the statistically significant difference between the VEGF content of output δ and output ϵ is likely attributable to the preferential concentration of microvesicles in output ϵ. Soluble VEGF contained within the conditioned medium primarily contributes to the VEGF readout in output δ, as compared to that of output ϵ, given the limited diffusion of this species across the device length (radius of gyration, $r_{\mathrm{g}}^{\mathrm{VEGF}} \approx 10\,\mathrm{nm}$; $l_{\mathrm{diffusion}} \approx 10\,\mu\mathrm{m}$).

Current extracellular shed vesicle and microvesicle harvesting approaches rely on centrifugation, filtration, and immunoaffinity. ESVs isolated by means of centrifugation, in which samples are pelleted (115, 165, 167, 183) or enriched (112), and immobilization (146, 167), in which ESVs are chemically-bound to an immunocoated surface, yield samples consisting of all species (*i.e.* exosomes and microvesicles) within the sample. By comparison, our microfluidic device yields a pure sample of intact microvesicles. As such, chemical analyses from our system, as compared to centrifugation or immobilization, represent components only expressed by microvesicles, instead of those expressed by all constituent ESVs. Filtration, in which off-the-shelf, low-protein-absorption $0.22\,\mu\mathrm{m}$ filters are typically used (21, 100, 114, 166), benefits from the serendipitous fact that the pore size aligns well with the natural gap (20) between small- and large-diameter ESV subpopulations. An attractive aspect of filtration is that it recovers and concentrates the resultant sample (21). Increasing pressure drops across filters, resulting from pores being filled by microvesicles, may damage the harvested population; to date, this phenomenon has not been quantified but a direct comparison between filter-concentrated microvesicles and microfluidic-concentrated microvesicles in future studies may clarify this. The current microfluidic device's most appealing aspects are its geometric tunability of threshold diameter and gentle treatment of ESVs, ensuring no ESV destruction or consolidation, and the demonstrated purity of the isolated micrdovesicles, and the confirmed difference in

protein content of separated ESV subpopulations. As this device does not concentrate vesicles, it has not demonstrated, to date, the sample volumes achieved via filtration and centrifugation (21, 115) for use in cell transformation assays or Western blots. Next-generation devices may address this by multiplying throughput.

4.5 Conclusions

Cancer-cell-derived ESVs, specifically microvesicles, are believed to play important roles in cancer progression including changing the behaviors of cells that make-up the tumor microenvironment in ways that drive primary tumor growth. ESVs, which as also shed into circulation, are believed to contribute to the priming of the metastatic niche. As cargo is believed to be correlated with size, it is important to isolate the large-diameter microvesicle population to identify unique cargoes and further establish microvesicles' role as a cancer biomarker. In this work, we developed a deterministic lateral displacement microfluidic device for the isolation of cancer-cell-derived microvesicles from conditioned medium containing a heterogeneous cancer-cell-derived extracellular shed vesicle population. We highlighted an exemplary case of chemical detection by measuring VEGF within each ESV-containing microfluidic output and showed a statistically-significant difference between the outputs, which likely results from microvesicle deflection to and concentration in the target output (ϵ). Additional chemical analyses could be conducted to measure other cargo of interest in on-going efforts to establish cancer-cell-derived microvesicles as cancer biomarkers and their role in cancer progression. The microfluidic device we designed and tested demonstrated a microvesicle-sized particle recovery efficiency of 39% with a corresponding purity of 98.5% in target output. The primary limitation of efficiency is attributable to the role of diffusion in the transport of such small particles. This

technology enables separation of microvesicle-sized particles and can be used to identify cargo carried by the microvesicle subpopulation. Such analyses could enable future investigations revealing microvesicles' provenance, functional activity, and mechanisms of transformation in cancer.

Acknowledgments

This work was supported by the National Cancer Institutes under under Award Number U54CA143876 and the Alfred P. Sloan Foundation.

CHAPTER 5

CONCLUSION

In this work I described and applied microfluidic devices to *(1)* enhance rare-cell, specifically CTC, microfluidic immunocapture systems and *(2)* isolate cancer-cell-derived MVs from samples containing heterogeneous ESV populations, and *(3)* characterized physical and chemical properties of cancer-cell-derived ESVs. These efforts seek to provide knowledge and tools that inform the study of cancer biology and cancer progression.

In chapter 2, I presented a study focused on tuning parameters for enhancing the target rare-cell capture within microfluidic immunocapture systems. The Hele-Shaw flow microfluidic device presented herein can be tuned to any fluid mechanical or chemical (*i.e.* antibody, aptamer, receptors) properties of interest to rare-cell isolation systems. We identified the ability to capture prostate cancer cells, using antibodies recognizing prostate specific membrane antigen, across a range of shear stresses relevant to microfluidic immunocapture platforms over a range of antibody concentrations. Furthermore this technique identified differential capture performance between two antibodies, J591 and J415, as a function of respective epitope location on the same target molecule. This system was established as a method for identifying the antibody types, targets, and composition, and shear stress, for enhanced rare-cell immunocapture for any rare-cell immunoaffinity system. Specifically in the case of prostate cancer, I determined a parameter space for enhanced isolation of patient-derived CTCs.

In chapter 3, I presented geometric and chemical characterization of cancer-cell-derived ESVs obtained from a number of cancerous epithelial cell lines sourced from brain, breast, and pancreatic cancers. In this investigation, I identified a bimodal ESV size distribution among ESVs harvested from each cancer cell line studied. Specifically, the large-diameter ESV, or microvesicle, population is present among only cancer cell types,

whereas the small-diameter, or exosome, population is present among all cell types studied, whether cancerous or normal epithelial. By applying a glutaminase inhibitor, compound 968, I determined that glutamine metabolism provides the energy necessary for MV production in cancer cells (PANC-1 and BxPC-3). Upon treatment with the glutaminase inhibitor, normal epithelial cells (hTERT-HPNE) experienced no change in total ESV production whereas cancerous epithelial cells experienced a nearly complete cessation of extracellular shed vesicle production, as measured by total ESV volume. These results bolster the claim that MVs represent a cancer-specific ESV subpopulation.

In chapter 4, I presented a novel microfluidic platform for the isolation of cancer-cell-derived MVs from a heterogeneous ESV population. Given the size-distribution data presented in chapter 3, I developed a determinisitic lateral displacement microfluidic platform that controls ESV trajectories as a function of diameter. This system resulted in the spatial separation of cancer-cell-derived MVs from exosomes with a threshold diameter of $250\,\mathrm{nm}$, which represents the diameter that distinguishes the exosome and MV subpopulations. This tool enables subsequent analyses regarding the provenance and formation of cancer-cell-derived ESV subpopulations to inform how they prepare the tumor microenvironment and sustain cancer progression.

Current ESV and MV harvesting approaches rely on centrifugation, filtration, and immunoaffinity. ESVs isolated by means of centrifugation yield samples consisting of all species (*i.e.* exosomes and microvesicles) within a sample with high recovery efficiency. ESVs harvested by means of filtration represent a pure microvesicle sample with high recovery efficiency. Both centrifugation and filtration approaches can concentrate ESVs harvested from a large volume. By comparison, our microfluidic device yields an intact microvesicle sample that is highly pure, and so performs similarly to filtration, but currently has low recovery efficiency and no on-device sample concentration.

Future work regarding microfluidic isolation of cancer-cell-derived MVs for use in a research context requires improving the following features: *(1)* more efficient sample recovery, *(2)* array modification to generate a pure exosome sample in addition to the pure microvesicle sample, *(3)* substantially increased total volume throughput, and *(4)* integration of a concentration stage following MV isolation. These modifications would yield samples with enough mass for chemical analysis or cell transformation assays, which motivate this work.

Additional device performance characterization is also recommended. Measuring the microdevice output-channel ESV content by means of dynamic light scattering following ESV-containing conditioned medium processing is required to describe this technology's ability to separate ESVs across the entire particle diameter range of interest. Following ESV separation performance, a panel of ELISA assays to identify cytosolic components, such as RhoC or IκBα, in addition to microvesicle-specific components, such as EGFR, EGFRvIII, or Flotillin-2, is recommended so as to identify the extent to which exosomes contaminate the microvesicle output. These assays would also identify cargo unique to microvesicles and not also expressed, in soluble form, in the conditioned medium, as is the case for VEGF.

Future work regarding to cancer-cell-derived ESV characterization, as described in chapter 3, should include a study focused on the role played by oncogenic RAS in total ESV production. In the reported work, differential total ESV volumes are reported among PANC-1, BxPC-3, and hTERT-HPNE cells; whereas PANC-1 and BxPC-3 cells are both cancerous pancreatic epithelial cell lines, only PANC-1 bears an oncogenic form of RAS. This observation is interesting given recent findings that RAS plays a central role in altering glutamine metabolism. These data indicate that RAS, and its associated downstream effector proteins, may play central roles in microvesicle production in cancer. This knowledge would inform questions regarding microvesicle

formation in cancer.

BIBLIOGRAPHY

[1] Christine L Chaffer and Robert A Weinberg. A perspective on cancer cell metastasis. *Science (New York, N.Y.)*, 331(6024):1559–64, March 2011.

[2] Héctor Peinado, Simon Lavotshkin, and David Lyden. The secreted factors responsible for pre-metastatic niche formation: old sayings and new thoughts. *Seminars in cancer biology*, 21(2):139–46, April 2011.

[3] Marina Bacac and Ivan Stamenkovic. Metastatic cancer cell. *Annual review of pathology*, 3:221–47, January 2008.

[4] Brian J Kirby, Mona Jodari, Matthew S Loftus, Gunjan Gakhar, Erica D Pratt, Chantal Chanel-Vos, Jason P Gleghorn, Steven M Santana, He Liu, James P Smith, Vicente N Navarro, Scott T Tagawa, Neil H Bander, David M Nanus, and Paraskevi Giannakakou. Functional characterization of circulating tumor cells with a prostate-cancer-specific microfluidic device. *PloS one*, 7(4):e35976, January 2012.

[5] Shannon L Stott, Chia-Hsien Hsu, Dina I Tsukrov, Min Yu, David T Miyamoto, Belinda A Waltman, S Michael Rothenberg, Ajay M Shah, Malgorzata E Smas, George K Korir, Frederick P Floyd, Anna J Gilman, Jenna B Lord, Daniel Winokur, Simeon Springer, Daniel Irimia, Sunitha Nagrath, Lecia V Sequist, Richard J Lee, Kurt J Isselbacher, Shyamala Maheswaran, Daniel A Haber, and Mehmet Toner. Isolation of circulating tumor cells using a microvortex-generating herringbone-chip. *Proceedings of the National Academy of Sciences*, 107:18392–18397, 2010.

[6] Erica D Pratt, Chao Huang, Benjamin G Hawkins, Jason P Gleghorn, and Brian J Kirby. Rare cell capture in microfluidic devices. *Chemical Engineering Science*, 66:1508–1522, 2011.

[7] Klaus Pantel and Catherine Alix-Panabières. Circulating tumour cells in cancer patients: challenges and perspectives. *Trends in molecular medicine*, 16:398–406, 2010.

[8] Shyamala Maheswaran and Daniel A Haber. Circulating tumor cells: a window into cancer biology and metastasis. *Current Opinion in Genetics & Development*, 20:96–99, 2010.

[9] Andrew D. Rhim, Fredrik I. Thege, Steven M. Santana, Timothy B. Lannin, Trisha N. Saha, Shannon Tsai, Lara R. Maggs, Michael L. Kochman, Gregory G. Ginsberg, John G. Lieb, Vinay Chandrasekhara, Jeffrey A. Drebin, Nuzhat Ahmad, Yu-Xiao Yang, Brian J. Kirby, and Ben Z. Stanger. Detection of Circulating Pancreas Epithelial Cells in Patients with Pancreatic Cystic Lesions. *Gastroenterology*, 2013.

[10] D C Danila, G Heller, G A Gignac, R Gonzalez-Espinoza, A Anand, E Tanaka, H Lilja, L Schwartz, S Larson, M Fleisher, and H I Scher. Circulating tumor cell number and prognosis in progressive castration-resistant prostate cancer. *Clinical cancer research : an official journal of the American Association for Cancer Research*, 13:7053–7058, 2007.

[11] Johann S de Bono, Howard I Scher, R B Montgomery, Christopher Parker, M C Miller, Henk Tissing, Gerald V Doyle, Leon W W M Terstappen, Kenneth J Pienta, and Derek Raghavan. Circulating tumor cells predict survival benefit from treatment in metastatic castration-resistant prostate cancer. *Clinical Cancer Research: An Official Journal Of The American Association For Cancer Research*, 14:6302–6309, January 2008.

[12] D Olmos, H T Arkenau, J E Ang, I Ledaki, G Attard, C P Carden, A H M Reid, R A'Hern, P C Fong, N B Oomen, R Molife, D Dearnaley, C Parker, L W

M M Terstappen, and J S de Bono. Circulating tumour cell (CTC) counts as intermediate end points in castration-resistant prostate cancer (CRPC): a single-centre experience. *Annals Of Oncology: Official Journal Of The European Society For Medical Oncology / ESMO*, 20:27–33, 2009.

[13] Andreas D. Hartkopf, Philipp Wagner, Diethelm Wallwiener, Tanja Fehm, and Ralf Rothmund. Changing Levels of Circulating Tumor Cells in Monitoring Chemotherapy Response in Patients with Metastatic Breast Cancer. *Anticancer Res*, 31(3):979–984, March 2011.

[14] Satoshi Matsusaka, Mitsukuni Suenaga, Yuji Mishima, Ryoko Kuniyoshi, Koichi Takagi, Yasuhito Terui, Nobuyuki Mizunuma, and Kiyohiko Hatake. Circulating tumor cells as a surrogate marker for determining response to chemotherapy in Japanese patients with metastatic colorectal cancer. *Cancer science*, 102(6):1188–92, June 2011.

[15] Gerhardt Attard, Joost F Swennenhuis, David Olmos, Alison H M Reid, Elaine Vickers, Roger A'Hern, Rianne Levink, Frank Coumans, Joana Moreira, Ruth Riisnaes, Nikhil Babu Oommen, George Hawche, Charles Jameson, Emilda Thompson, Ronald Sipkema, Craig P Carden, Christopher Parker, David Dearnaley, Stan B Kaye, Colin S Cooper, Arturo Molina, Michael E Cox, Leon W M M Terstappen, and Johann S de Bono. Characterization of ERG, AR and PTEN gene status in circulating tumor cells from patients with castration-resistant prostate cancer. *Cancer research*, 69:2912–2918, January 2009.

[16] Joost F Swennenhuis, Arjan G J Tibbe, Rianne Levink, Ronald C J Sipkema, and Leon W M M Terstappen. Characterization of circulating tumor cells by fluorescence in situ hybridization. *Cytometry Part A*, 75A:520–527, 2009.

[17] Ruth L Katz, Weigong He, Abha Khanna, Ricardo L Fernandez, Tanweer M

Zaidi, Matthew Krebs, Nancy P Caraway, Hua-Zhong Zhang, Feng Jiang, Margaret R Spitz, David P Blowers, Carlos A Jimenez, Reza J Mehran, Stephen G Swisher, Jack A Roth, Jeffrey S Morris, Carol J Etzel, and Randa El-Zein. Genetically abnormal circulating cells in lung cancer patients: an antigen-independent fluorescence in situ hybridization-based case-control study. *Clinical Cancer Research: An Official Journal Of The American Association For Cancer Research*, 16:3976–3987, January 2010.

[18] Ellen Heitzer, Martina Auer, Christin Gasch, Martin Pichler, Peter Ulz, Eva Maria Hoffmann, Sigurd Lax, Julie Waldispuehl-Geigl, Oliver Mauermann, Carolin Lackner, Gerald Höfler, Florian Eisner, Heinz Sill, Hellmut Samonigg, Klaus Pantel, Sabine Riethdorf, Thomas Bauernhofer, Jochen B Geigl, and Michael R Speicher. Complex tumor genomes inferred from single circulating tumor cells by array-CGH and next-generation sequencing. *Cancer research*, 73(10):2965–75, May 2013.

[19] Andrew D Rhim, Emily T Mirek, Nicole M Aiello, Anirban Maitra, Jennifer M Bailey, Florencia McAllister, Maximilian Reichert, Gregory L Beatty, Anil K Rustgi, Robert H Vonderheide, Steven D Leach, and Ben Z Stanger. EMT and dissemination precede pancreatic tumor formation. *Cell*, 148(1-2):349–61, January 2012.

[20] Steven M. Santana, Marc A. Antonyak, Richard A. Cerione, and Brian J. Kirby. Cancerous Epithelial Cell Lines Shed Extracellular Vesicles With a Bimodal Size Distribution that is Sensitive to Glutamine Inhibition. *Physical biology*, submitted, 2014.

[21] Marc A Antonyak, Bo Li, K Lindsey, Jared L Johnson, Joseph E Druso, Kirsten L Bryant, David A Holowka, Richard A. Cerione, and Lindsey K Boroughs.

Cancer cell-derived microvesicles induce transformation by transferring tissue transglutaminase and fibronectin to recipient cells. *Proceedings of the National Academy of Sciences*, 108(42):17569–17569, September 2011.

[22] Tae Hoon Lee, Esterina D'Asti, Nathalie Magnus, Khalid Al-Nedawi, Brian Meehan, and Janusz Rak. Microvesicles as mediators of intercellular communication in cancer–the emerging science of cellular 'debris'. *Seminars in immunopathology*, 33(5):455–67, September 2011.

[23] Xiao-Bo Li, Zhi-Ren Zhang, Hermann J. Schluesener, and Shun-Qing Xu. Role of exosomes in immune regulation. *Journal of Cellular and Molecular Medicine*, 10(2):364–375, April 2006.

[24] Vandhana Muralidharan-Chari, James W Clancy, Alanna Sedgwick, and Crislyn D'Souza-Schorey. Microvesicles: mediators of extracellular communication during cancer progression. *Journal of cell science*, 123(Pt 10):1603–11, May 2010.

[25] Suresh Mathivanan, Hong Ji, and Richard J Simpson. Exosomes: extracellular organelles important in intercellular communication. *Journal of proteomics*, 73:1907–1920, 2010.

[26] Angélique Bobrie, Marina Colombo, Graça Raposo, and Clotilde Théry. Exosome secretion: molecular mechanisms and roles in immune responses. *Traffic (Copenhagen, Denmark)*, 12(12):1659–68, December 2011.

[27] Cristina Grange, Marta Tapparo, Federica Collino, Loriana Vitillo, Christian Damasco, Maria Chiara Deregibus, Ciro Tetta, Benedetta Bussolati, and Giovanni Camussi. Microvesicles released from human renal cancer stem cells stimulate

angiogenesis and formation of lung premetastatic niche. *Cancer research*, 71(15):5346–56, August 2011.

[28] Johan Skog, Tom Würdinger, Sjoerd van Rijn, Dimphna H Meijer, Laura Gainche, Miguel Sena-Esteves, William T Curry, Bob S Carter, Anna M Krichevsky, and Xandra O Breakefield. Glioblastoma microvesicles transport RNA and proteins that promote tumour growth and provide diagnostic biomarkers. *Nature cell biology*, 10(12):1470–6, December 2008.

[29] Suresh Mathivanan and Richard J Simpson. ExoCarta: A compendium of exosomal proteins and RNA. *Proteomics*, 9(21):4997–5000, November 2009.

[30] Emanuele Cocucci, Gabriella Racchetti, and Jacopo Meldolesi. Shedding microvesicles: artefacts no more. *Trends in cell biology*, 19(2):43–51, February 2009.

[31] Marc A Antonyak, Kristin F Wilson, and Richard A. Cerione. R(h)oads to microvesicles. *Small GTPases*, 3(4):219–24, 2012.

[32] B Li, M A Antonyak, J Zhang, and Richard A. Cerione. RhoA triggers a specific signaling pathway that generates transforming microvesicles in cancer cells. *Oncogene*, 31(45):4740–9, November 2012.

[33] Khalid Al-Nedawi, Brian Meehan, Johann Micallef, Vladimir Lhotak, Linda May, Abhijit Guha, and Janusz Rak. Intercellular transfer of the oncogenic receptor EGFRvIII by microvesicles derived from tumour cells. *Nature cell biology*, 10(5):619–24, May 2008.

[34] Khalid Al-Nedawi, Brian Meehan, and Janusz Rak. Microvesicles: messengers and mediators of tumor progression. *Cell Cycle*, 8:2014–2018, 2009.

[35] Dolores Di Vizio, Matteo Morello, Andrew C Dudley, Peter W Schow, Rosalyn M Adam, Samantha Morley, David Mulholland, Mirja Rotinen, Martin H Hager, Luigi Insabato, Marsha A Moses, Francesca Demichelis, Michael P Lisanti, Hong Wu, Michael Klagsbrun, Neil A Bhowmick, Mark A Rubin, Crislyn D'Souza-Schorey, and Michael R Freeman. Large oncosomes in human prostate cancer tissues and in the circulation of mice with metastatic disease. *The American journal of pathology*, 181(5):1573–84, November 2012.

[36] Sascha Keller, Michael P Sanderson, Alexander Stoeck, and Peter Altevogt. Exosomes: From biogenesis and secretion to biological function. *Immunology Letters*, 107:102–108, 2006.

[37] Guillaume van Niel, Isabel Porto-Carreiro, Sabrina Simoes, and Graça Raposo. Exosomes: a common pathway for a specialized function. *Journal of biochemistry*, 140(1):13–21, July 2006.

[38] Wilhelm Schneiderhan, Fredy Diaz, Martin Fundel, Shaoxia Zhou, Marco Siech, Cornelia Hasel, Peter Möller, Jürgen E Gschwend, Thomas Seufferlein, Thomas Gress, Guido Adler, and Max G Bachem. Pancreatic stellate cells are an important source of MMP-2 in human pancreatic cancer and accelerate tumor progression in a murine xenograft model and CAM assay. *Journal of cell science*, 120(Pt 3):512–9, February 2007.

[39] Max G Bachem, Shaoxia Zhou, Karin Buck, Wilhelm Schneiderhan, and Marco Siech. Pancreatic stellate cells–role in pancreas cancer. *Langenbeck's archives of surgery / Deutsche Gesellschaft für Chirurgie*, 393(6):891–900, November 2008.

[40] Giovanni Camussi, Maria C Deregibus, Stefania Bruno, Vincenzo Cantaluppi, and Luigi Biancone. Exosomes/microvesicles as a mechanism of cell-to-cell communication. *Kidney international*, 78(9):838–48, November 2010.

[41] Ferdinando Pucci and Mikael J Pittet. Molecular pathways: tumor-derived microvesicles and their interactions with immune cells in vivo. *Clinical cancer research : an official journal of the American Association for Cancer Research*, 19(10):2598–604, May 2013.

[42] James P Smith, Alexander C Barbati, Steven M Santana, Jason P Gleghorn, and Brian J Kirby. Microfluidic transport in microdevices for rare cell capture. *Electrophoresis*, 33(21):3133–3142, November 2012.

[43] Chao Huang, Steven M Santana, He Liu, Neil H Bander, Benjamin G Hawkins, and Brian J Kirby. Characterization of a hybrid dielectrophoresis and immunocapture microfluidic system for cancer cell capture. *Electrophoresis*, 34(20-21):2970–9, November 2013.

[44] James P Smith, Timothy B Lannin, Yusef Syed, Steven M Santana, and Brian J Kirby. Parametric control of collision rates and capture rates in geometrically enhanced differential immunocapture (GEDI) microfluidic devices for rare cell capture. *Biomedical microdevices*, 16(1):143–51, February 2014.

[45] Giuseppe Galletti, Matthew S Sung, Linda T Vahdat, Manish A Shah, Steven M Santana, Giuseppe Altavilla, Brian J Kirby, and Paraskevi Giannakakou. Isolation of breast cancer and gastric cancer circulating tumor cells by use of an anti HER2-based microfluidic device. *Lab on a chip*, 14(1):147–56, January 2014.

[46] Steven M Santana, He Liu, Neil H Bander, Jason P Gleghorn, and Brian J Kirby. Immunocapture of prostate cancer cells by use of anti-PSMA antibodies in microdevices., April 2012.

[47] W Jeffrey Allard, Jeri Matera, M Craig Miller, Madeline Repollet, Mark C Connelly, Chandra Rao, Arjan G J Tibbe, Jonathan W Uhr, and Leon W M M

Terstappen. Tumor cells circulate in the peripheral blood of all major carcinomas but not in healthy subjects or patients with nonmalignant diseases. *Clinical Cancer Research: An Official Journal Of The American Association For Cancer Research*, 10:6897–6904, 2004.

[48] Robert T Krivacic, Andras Ladanyi, Douglas N Curry, H B Hsieh, Peter Kuhn, Danielle E Bergsrud, Jane F Kepros, Todd Barbera, Michael Y Ho, Lan Bo Chen, Richard A Lerner, and Richard H Bruce. A rare-cell detector for cancer. *Proceedings of the National Academy of Sciences of the United States of America*, 101:10501–10504, 2004.

[49] H I Scher, X Jia, J S de Bono, M Fleisher, K J Pienta, D Raghavan, and G Heller. Circulating tumour cells as prognostic markers in progressive, castration-resistant prostate cancer: a reanalysis of IMMC38 trial data. *The lancet oncology*, 10:233–239, 2009.

[50] F A W Coumans, C J M Doggen, G Attard, J S de Bono, and L W M M Terstappen. All circulating EpCAM+CK+CD45- objects predict overall survival in castration-resistant prostate cancer. *Annals of Oncology*, 21:1851–1857, 2010.

[51] Sunitha Nagrath, Lecia V Sequist, Shyamala Maheswaran, Daphne W Bell, Daniel Irimia, Lindsey Ulkus, Matthew R Smith, Eunice L Kwak, Subba Digumarthy, Alona Muzikansky, Paula Ryan, Ulysses J Balis, Ronald G Tompkins, Daniel A Haber, and Mehmet Toner. Isolation of rare circulating tumour cells in cancer patients by microchip technology. *Nature*, 450:1235–1239, 2007.

[52] Shannon L Stott, Richard J Lee, Sunitha Nagrath, Min Yu, David T Miyamoto, Lindsey Ulkus, Elizabeth J Inserra, Matthew Ulman, Simeon Springer, Zev Nakamura, Alessandra L Moore, Dina I Tsukrov, Maria E Kempner, Douglas M

Dahl, Chin-Lee Wu, A John Iafrate, Matthew R Smith, Ronald G Tompkins, Lecia V Sequist, Mehmet Toner, Daniel A Haber, and Shyamala Maheswaran. Isolation and Characterization of Circulating Tumor Cells from Patients with Localized and Metastatic Prostate Cancer. *Science Translational Medicine*, 2:25ra23, 2010.

[53] Sabine Riethdorf and Klaus Pantel. Advancing personalized cancer therapy by detection and characterization of circulating carcinoma cells Circulating tumor cells in cancer patients Riethdorf & Pantel. *Annals of the New York Academy of Sciences*, 1210:66–77, 2010.

[54] Jose G Moreno, M Craig Miller, Steve Gross, W Jeffrey Allard, Leonard G Gomella, and Leon W M M Terstappen. Circulating tumor cells predict survival in patients with metastatic prostate cancer. *Urology*, 65:713–718, 2005.

[55] Steven J Cohen, Cornelis J A Punt, Nicholas Iannotti, Bruce H Saidman, Kert D Sabbath, Nashat Y Gabrail, Joel Picus, Michael Morse, Edith Mitchell, M Craig Miller, Gerald V Doyle, Henk Tissing, Leon W M M Terstappen, and Neal J Meropol. Relationship of Circulating Tumor Cells to Tumor Response, Progression-Free Survival, and Overall Survival in Patients With Metastatic Colorectal Cancer. *Journal of Clinical Oncology*, 26:3213–3221, 2008.

[56] Shine-Gwo Shiah, Kang-Yu Tai, and Cheng-Wen Wu. Epigenetic regulation of EpCAM in tumor invasion and metastasis. *J. Cancer Mol.*, 3(6):165–168, 2008.

[57] Markus Munz, Patrick A Baeuerle, and Olivier Gires. The Emerging Role of EpCAM in Cancer and Stem Cell Signaling. *Cancer research*, 69:5627–5629, 2009.

[58] Johanna Gostner, Dominic Fong, Oliver Wrulich, Florian Lehne, Marion Zitt,

Martin Hermann, Sylvia Krobitsch, Agnieszka Martowicz, Guenther Gastl, and Gilbert Spizzo. Effects of EpCAM overexpression on human breast cancer cell lines. *BMC Cancer*, 11:45, 2011.

[59] M Mego, U De Giorgi, L Hsu, N T Ueno, V Valero, S Jackson, E Andreopoulou, S.-W. Kau, J M Reuben, and M Cristofanilli. Circulating tumor cells in metastatic inflammatory breast cancer. *Annals of Oncology*, 20:1824–1828, 2009.

[60] Angela Gradilone, Cristina Raimondi, Chiara Nicolazzo, Arianna Petracca, Orietta Gandini, Bruno Vincenzi, Giuseppe Naso, Anna Maria Aglianò, Enrico Cortesi, and Paola Gazzaniga. Circulating tumor cells lacking cytokeratin in breast cancer: the importance of being mesenchymal. *Journal of Cellular and Molecular Medicine*, pages no–no, 2011.

[61] H Liu, P Moy, S Kim, Y Xia, A Rajasekaran, V Navarro, B Knudsen, and N H Bander. Monoclonal antibodies to the extracellular domain of prostate-specific membrane antigen also react with tumor vascular endothelium. *Cancer research*, 57:3629–3634, 1997.

[62] Sam S Chang, Victor E Reuter, W D W Heston, Neil H Bander, Lana S Grauer, and Paul B Gaudin. Five Different Anti-Prostate-specific Membrane Antigen (PSMA) Antibodies Confirm PSMA Expression in Tumor-associated Neovasculature. *Cancer research*, 59:3192–3198, 1999.

[63] Neil H Bander, David M Nanus, Matthew I Milowsky, Lale Kostakoglu, Shankar Vallabahajosula, and Stanley J Goldsmith. Targeted systemic therapy of prostate cancer with a monoclonal antibody to prostate-specific membrane antigen. *Seminars in oncology*, 30:667–676, 2003.

[64] Mindy I Davis, Melanie J Bennett, Leonard M Thomas, and Pamela J Bjorkman.

Crystal structure of prostate-specific membrane antigen, a tumor marker and peptidase. *Proceedings of the National Academy of Sciences of the United States of America*, 102:5981–5986, 2005.

[65] George L Wright, Cara Haley, Mary Lou Beckett, and Paul F Schellhammer. Expression of prostate-specific membrane antigen in normal, benign, and malignant prostate tissues. *Urologic Oncology: Seminars and Original Investigations*, 1:18–28, 1995.

[66] Gerald P Murphy, Abdel-Aziz A Elgamal, Sai L Su, David G Bostwick, and Eric H Holmes. Current evaluation of the tissue localization and diagnostic utility of prostate specific membrane antigen. *Cancer*, 83:2259–2269, 1998.

[67] Tomomi Kusumi, Takuya Koie, Masanori Tanaka, Kazuhito Matsumoto, Fuyuki Sato, Akinori Kusumi, Chikara Ohyama, and Hiroshi Kijima. Immunohistochemical detection of carcinoma in radical prostatectomy specimens following hormone therapy. *Pathology International*, 58:687–694, 2008.

[68] Sebastian Mannweiler, Peter Amersdorfer, Slave Trajanoski, Jonathan Terrett, David King, and Gabor Mehes. Heterogeneity of Prostate-Specific Membrane Antigen (PSMA) Expression in Prostate Carcinoma with Distant Metastasis. *Pathology & Oncology Research*, 15:167–172, 2009.

[69] S S Chang, D S O'Keefe, D J Bacich, V E Reuter, W D Heston, and P B Gaudin. Prostate-specific membrane antigen is produced in tumor-associated neovasculature. *Clinical cancer research : an official journal of the American Association for Cancer Research*, 5:2674–2681, 1999.

[70] Ron S Israeli, Wilson H Miller, Sai L Su, C Thomas Powell, William R Fair, Dan S Samadi, Robert F Huryk, Anthony DeBlasio, Elizabeth T

Edwards, Gilbert J Wise, and Warren D W Heston. Sensitive Nested Reverse Transcription Polymerase Chain Reaction Detection of Circulating Prostatic Tumor Cells: Comparison of Prostate-specific Membrane Antigen and Prostate-specific Antigen-based Assays. *Cancer research*, 54:6306–6310, 1994.

[71] George L Wright, B Mayer Grob, Cara Haley, Katie Grossman, Kathy Newhall, Daniel Petrylak, John Troyer, Alice Konchuba, Paul F Schellhammer, and Richard Moriarty. Upregulation of prostate-specific membrane antigen after androgen-deprivation therapy. *Urology*, 48:326–334, 1996.

[72] Susan D Sweat, Anna Pacelli, Gerald P Murphy, and David G Bostwick. Prostate-specific membrane antigen expression is greatest in prostate adenocarcinoma and lymph node metastases. *Urology*, 52:637–640, 1998.

[73] Jeffrey S Ross, Christine E Sheehan, Hugh A G Fisher, Ronald P Kaufman, Prabhjot Kaur, Karen Gray, Iain Webb, Gary S Gray, Rebecca Mosher, and Bhaskar V S Kallakury. Correlation of Primary Tumor Prostate-Specific Membrane Antigen Expression with Disease Recurrence in Prostate Cancer. *Clinical Cancer Research*, 9:6357–6362, 2003.

[74] Sven Perner, Matthias D Hofer, Robert Kim, Rajal B Shah, Haojie Li, Peter Möller, Richard E Hautmann, Juergen E Gschwend, Rainer Kuefer, and Mark A Rubin. Prostate-specific membrane antigen expression as a predictor of prostate cancer progression. *Human Pathology*, 38:696–701, 2007.

[75] S Minner, C Wittmer, M Graefen, G Salomon, T Steuber, A Haese, H Huland, C Bokemeyer, E Yekebas, J Dierlamm, S Balabanov, E Kilic, W Wilczak, R Simon, G Sauter, and T Schlomm. High level PSMA expression is associated with early PSA recurrence in surgically treated prostate cancer. *The Prostate*, 71:281–288, 2011.

[76] J P Gleghorn, E D Pratt, D Denning, H Liu, N H Bander, S T Tagawa, D M Nanus, P A Giannakakou, and B J Kirby. Capture of circulating tumor cells from whole blood of prostate cancer patients using geometrically enhanced differential immunocapture (GEDI) and a prostate-specific antibody. *Lab on a chip*, 10:27–29, 2010.

[77] S K Murthy, A Sin, R G Tompkins, and M Toner. Effect of Flow and Surface Conditions on Human Lymphocyte Isolation Using Microfluidic Chambers. *Langmuir : the ACS journal of surfaces and colloids.*, 20:11649, 2004.

[78] S Usami, H H Chen, Y Zhao, S Chien, and R Skalak. Design and construction of a linear shear stress flow chamber. *Annals of Biomedical Engineering*, 21:77–83, 1993.

[79] Aaron Sin, Shashi K Murthy, Alexander Revzin, Ronald G Tompkins, and Mehmet Toner. Enrichment using antibody-coated microfluidic chambers in shear flow: Model mixtures of human lymphocytes. *Biotechnology and Bioengineering*, 91:816–826, 2005.

[80] Brian J Kirby, Aaron R Wheeler, Richard N Zare, Julia A Fruetel, and Timothy J Shepodd. Programmable modification of cell adhesion and zeta potential in silica microchips. *Lab on a chip*, 3:5–10, 2003.

[81] Daniel C Danila, Martin Fleisher, and Howard I Scher. Circulating tumor cells as biomarkers in prostate cancer. *Clinical cancer research : an official journal of the American Association for Cancer Research*, 17(12):3903–12, June 2011.

[82] D A Silver, I Pellicer, W R Fair, W D Heston, and C Cordon-Cardo. Prostate-specific membrane antigen expression in normal and malignant human tissues. *Clinical Cancer Research*, 3:81–85, 1997.

[83] Michael C Haffner, Irmgard E Kronberger, Jeffrey S Ross, Christine E Sheehan, Matthias Zitt, Gilbert MÃhlmann, Dietmar Ãfner, Bettina Zelger, Christian Ensinger, Ximing J Yang, Stephan Geley, Raimund Margreiter, and Neil H Bander. Prostate-specific membrane antigen expression in the neovasculature of gastric and colorectal cancers. *Human Pathology*, 40:1754–1761, 2009.

[84] J S Horoszewicz, E Kawinski, and G P Murphy. Monoclonal antibodies to a new antigenic marker in epithelial prostatic cells and serum of prostatic cancer patients. *Anticancer research*, 7(5B):927–35, January 1987.

[85] Ron S Israeli, C Thomas Powell, John G Corr, William R Fair, and Warren D W Heston. Expression of the Prostate-specific Membrane Antigen. *Cancer research*, 54:1807–1811, 1994.

[86] John K Trover, Mary Lou Beckett, and George L Wright. Detection and characterization of the prostate-specific membrane antigen (PSMA) in tissue extracts and body fluids. *International Journal of Cancer*, 62:552–558, 1995.

[87] R L Sokoloff, K C Norton, C L Gasior, K M Marker, and L S Grauer. A dual-monoclonal sandwich assay for prostate-specific membrane antigen: Levels in tissues, seminal fluid and urine. *The Prostate*, 43:150–157, 2000.

[88] Ayyappan K Rajasekaran, Gopalakrishnapillai Anilkumar, and Jason J Christiansen. Is prostate-specific membrane antigen a multifunctional protein? *American Journal of Physiology - Cell Physiology*, 288(5):C975–C981, May 2005.

[89] Peter M Smith-Jones, Shankar Vallabahajosula, Stanley J Goldsmith, Vincent Navarro, Catherine J Hunter, Diego Bastidas, and Neil H Bander. In Vitro Characterization of Radiolabeled Monoclonal Antibodies Specific for the

Extracellular Domain of Prostate-specific Membrane Antigen. *Cancer research*, 60:5237–5243, 2000.

[90] Jeroen R Mesters, Cyril Barinka, Weixing Li, Takashi Tsukamoto, Pavel Majer, Barbara S Slusher, Jan Konvalinka, and Rolf Hilgenfeld. Structure of glutamate carboxypeptidase II, a drug target in neuronal damage and prostate cancer. *The EMBO journal*, 25(6):1375–84, March 2006.

[91] Feng Guo, Jarrod B French, Peng Li, Hong Zhao, Chung Yu Chan, James R Fick, Stephen J Benkovic, and Tony Jun Huang. Probing cell-cell communication with microfluidic devices. *Lab on a chip*, 13(16):3152–62, August 2013.

[92] C Harding, J Heuser, and P Stahl. Endocytosis and intracellular processing of transferrin and colloidal gold-transferrin in rat reticulocytes: demonstration of a pathway for receptor shedding. *European journal of cell biology*, 35(2):256–63, November 1984.

[93] B. T. Pan. Electron microscopic evidence for externalization of the transferrin receptor in vesicular form in sheep reticulocytes. *The Journal of Cell Biology*, 101(3):942–948, September 1985.

[94] R M Johnstone, M Adam, J R Hammond, L Orr, and C Turbide. Vesicle formation during reticulocyte maturation. Association of plasma membrane activities with released vesicles (exosomes). *J. Biol. Chem.*, 262(19):9412–9420, July 1987.

[95] C. Friend, W. Marovitz, G. Henle, W. Henle, D. Tsuei, K. Hirschhorn, J. G. Holland, and J. Cuttner. Observations on Cell Lines Derived from a Patient with Hodgkin's Disease. *Cancer Res.*, 38(8):2581–2591, August 1978.

[96] Rose M Johnstone. Exosomes biological significance: a concise review. *Blood Cells, Molecules, and Diseases*, 36(2):315–21, April 2006.

[97] M Iero, R Valenti, V Huber, P Filipazzi, G Parmiani, S Fais, and L Rivoltini. Tumour-released exosomes and their implications in cancer immunity. *Cell death and differentiation*, 15(1):80–8, January 2008.

[98] F F Van Doormaal, A Kleinjan, M Di Nisio, H R Büller, and R Nieuwland. Cell-derived microvesicles and cancer. *Neth J Med*, 67(7):266–273, 2009.

[99] Jeffrey S Schorey and Sanchita Bhatnagar. Exosome function: from tumor immunology to pathogen biology. *Traffic*, 9:871–881, 2008.

[100] Richard J Simpson, Justin We E Lim, Robert L Moritz, and Suresh Mathivanan. Exosomes: proteomic insights and diagnostic potential. *Expert review of proteomics*, 6(3):267–83, June 2009.

[101] Donatello Castellana, Florence Toti, and Jean-Marie Freyssinet. Membrane microvesicles: Macromessengers in cancer disease and progression. *Thrombosis Research*, 125, Suppl:S84–S88, 2010.

[102] Crislyn D'Souza-Schorey and James W Clancy. Tumor-derived microvesicles: shedding light on novel microenvironment modulators and prospective cancer biomarkers. *Genes & development*, 26(12):1287–99, June 2012.

[103] Douglas D Taylor and Cicek Gercel-Taylor. Exosomes/microvesicles: mediators of cancer-associated immunosuppressive microenvironments. *Seminars in immunopathology*, 33(5):441–54, September 2011.

[104] Maarten E Tushuizen, Michaela Diamant, Augueste Sturk, and Rienk Nieuwland. Cell-derived microparticles in the pathogenesis of cardiovascular disease: friend or foe? *Arteriosclerosis, thrombosis, and vascular biology*, 31(1):4–9, January 2011.

[105] Matteo Morello, Valentina R Minciacchi, Paola de Candia, Julie Yang, Edwin Posadas, Hyung Kim, Duncan Griffiths, Neil Bhowmick, Leland WK Chung, Paolo Gandellini, Michael R Freeman, Francesca Demichelis, and Dolores Di Vizio. Large oncosomes mediate intercellular transfer of functional microRNA. *Cell Cycle*, 12(22):59–69, November 2013.

[106] Edgardo V. Ariztia, Catherine J. Lee, Radhika Gogoi, and David A. Fishman. The Tumor Microenvironment: Key to Early Detection. *Critical reviews in clinical laboratory sciences*, 43(5-6):393–425, October 2008.

[107] Jung Eun Park, Hon Sen Tan, Arnab Datta, Ruenn Chai Lai, Huoming Zhang, Wei Meng, Sai Kiang Lim, and Siu Kwan Sze. Hypoxic tumor cell modulates its microenvironment to enhance angiogenic and metastatic potential by secretion of proteins and exosomes. *Molecular & cellular proteomics : MCP*, 9(6):1085–99, June 2010.

[108] Bethan Psaila and David Lyden. The metastatic niche: adapting the foreign soil. *Nature reviews. Cancer*, 9(4):285–93, April 2009.

[109] Hyungsoon Im, Huilin Shao, Yong Il Park, Vanessa M Peterson, Cesar M Castro, Ralph Weissleder, and Hakho Lee. Label-free detection and molecular profiling of exosomes with a nano-plasmonic sensor. *Nature biotechnology*, 32(5):490–5, May 2014.

[110] C Théry, M Boussac, P Véron, P Ricciardi-Castagnoli, G Raposo, J Garin, and S Amigorena. Proteomic analysis of dendritic cell-derived exosomes: a secreted subcellular compartment distinct from apoptotic vesicles. *Journal of immunology (Baltimore, Md. : 1950)*, 166(12):7309–18, June 2001.

[111] Hadi Valadi, Karin Ekström, Apostolos Bossios, Margareta Sjöstrand, James J

Lee, and Jan O Lötvall. Exosome-mediated transfer of mRNAs and microRNAs is a novel mechanism of genetic exchange between cells. *Nature cell biology*, 9(6):654–9, June 2007.

[112] Dong-Sic Choi, Jae-Min Lee, Gun Wook Park, Hyeon-Woo Lim, Joo Young Bang, Yoon-Keun Kim, Kyung-Hoon Kwon, Ho Jeong Kwon, Kwang Pyo Kim, and Yong Song Gho. Proteomic analysis of microvesicles derived from human colorectal cancer cells. *Journal of proteome research*, 6(12):4646–55, December 2007.

[113] Y Yuana, T H Oosterkamp, S Bahatyrova, B Ashcroft, P Garcia Rodriguez, R M Bertina, and S Osanto. Atomic force microscopy: a novel approach to the detection of nanosized blood microparticles. *Journal of thrombosis and haemostasis : JTH*, 8(2):315–23, February 2010.

[114] A S Lawrie, A Albanyan, R A Cardigan, I J Mackie, and P Harrison. Microparticle sizing by dynamic light scattering in fresh-frozen plasma. *Vox sanguinis*, 96(3):206–12, April 2009.

[115] Malene Jorgensen, Rikke Baek, Shona Pedersen, Evo K.L. Sondergaard, Soren R. Kristensen, and Kim Varming. Extracellular Vesicle (EV) Array: microarray capturing of exosomes and other extracellular vesicles for multiplexed phenotyping. *Journal of Extracellular Vesicles*, 2, 2013.

[116] E van der Pol, A G Hoekstra, A Sturk, C Otto, T G van Leeuwen, and R Nieuwland. Optical and non-optical methods for detection and characterization of microparticles and exosomes. *Journal of thrombosis and haemostasis : JTH*, 8(12):2596–607, December 2010.

[117] J Ratajczak, M Wysoczynski, F Hayek, A Janowska-Wieczorek, and M Z

Ratajczak. Membrane-derived microvesicles: important and underappreciated mediators of cell-to-cell communication. *Leukemia*, 20(9):1487–1495, September 2006.

[118] Shengming Dai, Dong Wei, Zhen Wu, Xiangyang Zhou, Xiaomou Wei, Haixin Huang, and Guisheng Li. Phase I clinical trial of autologous ascites-derived exosomes combined with GM-CSF for colorectal cancer. *Molecular therapy : the journal of the American Society of Gene Therapy*, 16(4):782–90, April 2008.

[119] Bernard Escudier, Thierry Dorval, Nathalie Chaput, Fabrice André, Marie-Pierre Caby, Sophie Novault, Caroline Flament, Christophe Leboulaire, Christophe Borg, Sebastian Amigorena, Catherine Boccaccio, Christian Bonnerot, Olivier Dhellin, Mojgan Movassagh, Sophie Piperno, Caroline Robert, Vincent Serra, Nancy Valente, Jean-Bernard Le Pecq, Alain Spatz, Olivier Lantz, Thomas Tursz, Eric Angevin, and Laurence Zitvogel. Vaccination of metastatic melanoma patients with autologous dendritic cell (DC) derived-exosomes: results of thefirst phase I clinical trial. *Journal of translational medicine*, 3(1):10, March 2005.

[120] Sophie Viaud, Clotilde Théry, Stéphanie Ploix, Thomas Tursz, Valérie Lapierre, Olivier Lantz, Laurence Zitvogel, and Nathalie Chaput. Dendritic cell-derived exosomes for cancer immunotherapy: what's next? *Cancer research*, 70(4):1281–5, February 2010.

[121] Bence György, Károly Módos, Eva Pállinger, Krisztina Pálóczi, Mária Pásztói, Petra Misják, Mária A Deli, Aron Sipos, Anikó Szalai, István Voszka, Anna Polgár, Kálmán Tóth, Mária Csete, György Nagy, Steffen Gay, András Falus, Agnes Kittel, and Edit I Buzás. Detection and isolation of cell-derived microparticles are compromised by protein complexes resulting from shared biophysical parameters. *Blood*, 117(4):e39–48, January 2011.

[122] Rebecca Siegel, Deepa Naishadham, and Ahmedin Jemal. Cancer statistics, 2012. *CA: a cancer journal for clinicians*, 62(1):10–29, 2012.

[123] DavidA. Tuveson and JohnP. Neoptolemos. Understanding Metastasis in Pancreatic Cancer: A Call for New Clinical Approaches. *Cell*, 148(1):21–23, 2012.

[124] Stefan Eser, Marlena Messer, Philipp Eser, Alexander von Werder, Barbara Seidler, Monther Bajbouj, Roger Vogelmann, Alexander Meining, Johannes von Burstin, Hana Algül, Philipp Pagel, Angelika E Schnieke, Irene Esposito, Roland M Schmid, Günter Schneider, and Dieter Saur. In vivo diagnosis of murine pancreatic intraepithelial neoplasia and early-stage pancreatic cancer by molecular imaging. *Proceedings of the National Academy of Sciences of the United States of America*, 108(24):9945–50, June 2011.

[125] Aram F Hezel, Alec C Kimmelman, Ben Z Stanger, Nabeel Bardeesy, and Ronald A Depinho. Genetics and biology of pancreatic ductal adenocarcinoma. *Genes & development*, 20(10):1218–49, May 2006.

[126] Marina Pasca di Magliano and Craig D. Logsdon. Roles for KRAS in Pancreatic Tumor Development and Progression. *Gastroenterology*, 144(6):1220–1229, 2013.

[127] Alberto Fernández-Medarde and Eugenio Santos. Ras in cancer and developmental diseases. *Genes & cancer*, 2(3):344–58, March 2011.

[128] M Spaargaren, J R Bischoff, and F McCormick. Signal transduction by Ras-like GTPases: a potential target for anticancer drugs. *Gene expression*, 4(6):345–56, January 1995.

[129] Andrew V Biankin, Nicola Waddell, Karin S Kassahn, Marie-Claude Gingras, Lakshmi B Muthuswamy, Amber L Johns, David K Miller, Peter J Wilson, Ann-Marie Patch, Jianmin Wu, David K Chang, Mark J Cowley, Brooke B Gardiner, Sarah Song, Ivon Harliwong, Senel Idrisoglu, Craig Nourse, Ehsan Nourbakhsh, Suzanne Manning, Shivangi Wani, Milena Gongora, Marina Pajic, Christopher J Scarlett, Anthony J Gill, Andreia V Pinho, Ilse Rooman, Matthew Anderson, Oliver Holmes, Conrad Leonard, Darrin Taylor, Scott Wood, Qinying Xu, Katia Nones, J Lynn Fink, Angelika Christ, Tim Bruxner, Nicole Cloonan, Gabriel Kolle, Felicity Newell, Mark Pinese, R Scott Mead, Jeremy L Humphris, Warren Kaplan, Marc D Jones, Emily K Colvin, Adnan M Nagrial, Emily S Humphrey, Angela Chou, Venessa T Chin, Lorraine A Chantrill, Amanda Mawson, Jaswinder S Samra, James G Kench, Jessica A Lovell, Roger J Daly, Neil D Merrett, Christopher Toon, Krishna Epari, Nam Q Nguyen, Andrew Barbour, Nikolajs Zeps, Nipun Kakkar, Fengmei Zhao, Yuan Qing Wu, Min Wang, Donna M Muzny, William E Fisher, F Charles Brunicardi, Sally E Hodges, Jeffrey G Reid, Jennifer Drummond, Kyle Chang, Yi Han, Lora R Lewis, Huyen Dinh, Christian J Buhay, Timothy Beck, Lee Timms, Michelle Sam, Kimberly Begley, Andrew Brown, Deepa Pai, Ami Panchal, Nicholas Buchner, Richard De Borja, Robert E Denroche, Christina K Yung, Stefano Serra, Nicole Onetto, Debabrata Mukhopadhyay, Ming-Sound Tsao, Patricia A Shaw, Gloria M Petersen, Steven Gallinger, Ralph H Hruban, Anirban Maitra, Christine A Iacobuzio-Donahue, Richard D Schulick, Christopher L Wolfgang, Richard A Morgan, Rita T Lawlor, Paola Capelli, Vincenzo Corbo, Maria Scardoni, Giampaolo Tortora, Margaret A Tempero, Karen M Mann, Nancy A Jenkins, Pedro A Perez-Mancera, David J Adams, David A Largaespada, Lodewyk F A Wessels, Alistair G Rust, Lincoln D Stein, David A Tuveson,

Neal G Copeland, Elizabeth A Musgrove, Aldo Scarpa, James R Eshleman, Thomas J Hudson, Robert L Sutherland, David A Wheeler, John V Pearson, John D McPherson, Richard A Gibbs, and Sean M Grimmond. Pancreatic cancer genomes reveal aberrations in axon guidance pathway genes. *Nature*, 491(7424):399–405, November 2012.

[130] Siân Jones, Xiaosong Zhang, D Williams Parsons, Jimmy Cheng-Ho Lin, Rebecca J Leary, Philipp Angenendt, Parminder Mankoo, Hannah Carter, Hirohiko Kamiyama, Antonio Jimeno, Seung-Mo Hong, Baojin Fu, Ming-Tseh Lin, Eric S Calhoun, Mihoko Kamiyama, Kimberly Walter, Tatiana Nikolskaya, Yuri Nikolsky, James Hartigan, Douglas R Smith, Manuel Hidalgo, Steven D Leach, Alison P Klein, Elizabeth M Jaffee, Michael Goggins, Anirban Maitra, Christine Iacobuzio-Donahue, James R Eshleman, Scott E Kern, Ralph H Hruban, Rachel Karchin, Nickolas Papadopoulos, Giovanni Parmigiani, Bert Vogelstein, Victor E Velculescu, and Kenneth W Kinzler. Core signaling pathways in human pancreatic cancers revealed by global genomic analyses. *Science (New York, N.Y.)*, 321(5897):1801–6, September 2008.

[131] Jaekyoung Son, Costas A Lyssiotis, Haoqiang Ying, Xiaoxu Wang, Sujun Hua, Matteo Ligorio, Rushika M Perera, Cristina R Ferrone, Edouard Mullarky, Ng Shyh-Chang, Ya'an Kang, Jason B Fleming, Nabeel Bardeesy, John M Asara, Marcia C Haigis, Ronald A DePinho, Lewis C Cantley, and Alec C Kimmelman. Glutamine supports pancreatic cancer growth through a KRAS-regulated metabolic pathway. *Nature*, 496(7443):101–5, April 2013.

[132] Haoqiang Ying, AlecC. Kimmelman, CostasA. Lyssiotis, Sujun Hua, GeraldC. Chu, Eliot Fletcher-Sananikone, JasonW. Locasale, Jaekyoung Son, Hailei Zhang, JonathanL. Coloff, Haiyan Yan, Wei Wang, Shujuan Chen, Andrea Viale,

Hongwu Zheng, Ji-hye Paik, Carol Lim, AlexanderR. Guimaraes, EricS. Martin, Jeffery Chang, AramF. Hezel, SamuelR. Perry, Jian Hu, Boyi Gan, Yonghong Xiao, JohnM. Asara, Ralph Weissleder, Y.Alan Wang, Lynda Chin, LewisC. Cantley, and RonaldA. DePinho. Oncogenic Kras Maintains Pancreatic Tumors through Regulation of Anabolic Glucose Metabolism. *Cell*, 149(3):656–670, 2012.

[133] Costas A Lyssiotis, Jaekyoung Son, Lewis C Cantley, and Alec C Kimmelman. Pancreatic cancers rely on a novel glutamine metabolism pathway to maintain redox balance. *Cell cycle (Georgetown, Tex.)*, 12(13):1987–8, July 2013.

[134] PatrickS. Ward and CraigB. Thompson. Metabolic Reprogramming: A Cancer Hallmark Even Warburg Did Not Anticipate. *Cancer Cell*, 21(3):297–308, 2012.

[135] Peggy P. Hsu and David M. Sabatini. Cancer Cell Metabolism: Warburg and Beyond. *Cell*, 134(5):703–7, September 2008.

[136] Matthew G Vander Heiden, Lewis C Cantley, and Craig B Thompson. Understanding the Warburg effect: the metabolic requirements of cell proliferation. *Science (New York, N.Y.)*, 324(5930):1029–33, May 2009.

[137] David R. Wise and Craig B. Thompson. Glutamine addiction: a new therapeutic target in cancer. *Trends in Biochemical Sciences*, 35(8):427–433, 2010.

[138] Jason R Cantor and David M Sabatini. Cancer cell metabolism: one hallmark, many faces. *Cancer discovery*, 2(10):881–98, October 2012.

[139] Mohan R Kaadige, Ryan E Looper, Sadhaasivam Kamalanaadhan, and Donald E Ayer. Glutamine-dependent anapleurosis dictates glucose uptake and cell growth by regulating MondoA transcriptional activity. *Proceedings of the National*

Academy of Sciences of the United States of America, 106(35):14878–83, September 2009.

[140] Elizabeth J Sloan and Donald E Ayer. Myc, mondo, and metabolism. *Genes & cancer*, 1(6):587–96, June 2010.

[141] Nicola Montano, Tonia Cenci, Maurizio Martini, Quintino Giorgio D'Alessandris, Federica Pelacchi, Lucia Ricci-Vitiani, Giulio Maira, Ruggero De Maria, Luigi Maria Larocca, and Roberto Pallini. Expression of EGFRvIII in glioblastoma: prognostic significance revisited. *Neoplasia (New York, N.Y.)*, 13(12):1113–21, December 2011.

[142] Huilin Shao, Jaehoon Chung, Leonora Balaj, Alain Charest, Darell D Bigner, Bob S Carter, Fred H Hochberg, Xandra O Breakefield, Ralph Weissleder, and Hakho Lee. Protein typing of circulating microvesicles allows real-time monitoring of glioblastoma therapy. *Nature medicine*, 18(12):1835–40, December 2012.

[143] Jian-Bin Wang, Jon W. Erickson, Reina Fuji, Sekar Ramachandran, Ping Gao, Ramani Dinavahi, Kristin F. Wilson, Andre L.B. Ambrosio, Sandra M.G. Dias, Chi V. Dang, and Richard A. Cerione. Targeting Mitochondrial Glutaminase Activity Inhibits Oncogenic Transformation. *Cancer Cell*, 18(3):207–219, 2010.

[144] William P Katt, Sekar Ramachandran, Jon W Erickson, and Richard A. Cerione. Dibenzophenanthridines as inhibitors of glutaminase C and cancer cell proliferation. *Molecular cancer therapeutics*, 11(6):1269–78, June 2012.

[145] Edwin van der Pol, Anita N Böing, Paul Harrison, Augueste Sturk, and Rienk Nieuwland. Classification, functions, and clinical relevance of extracellular vesicles. *Pharmacological reviews*, 64(3):676–705, July 2012.

[146] Lori V Coren, Teresa Shatzer, and David E Ott. CD45 immunoaffinity depletion of vesicles from Jurkat T cells demonstrates that exosomes contain CD45: no evidence for a distinct exosome/HIV-1 budding pathway. *Retrovirology*, 5(1):64, January 2008.

[147] E A Clark, T R Golub, E S Lander, and R O Hynes. Genomic analysis of metastasis reveals an essential role for RhoC. *Nature*, 406(6795):532–5, August 2000.

[148] Ulrike Kutay, Christos Stournaras, Francisco M. Vega, and Anne J. Ridley. Rho GTPases in cancer cell biology. *FEBS Letters*, 582(14):2093–2101, 2008.

[149] Chi V Dang. MYC, microRNAs and glutamine addiction in cancers. *Cell cycle (Georgetown, Tex.)*, 8(20):3243–5, October 2009.

[150] Bence György, Tamás G Szabó, Mária Pásztói, Zsuzsanna Pál, Petra Misják, Borbála Aradi, Valéria László, Eva Pállinger, Erna Pap, Agnes Kittel, György Nagy, András Falus, and Edit I Buzás. Membrane vesicles, current state-of-the-art: emerging role of extracellular vesicles. *Cellular and molecular life sciences : CMLS*, 68(16):2667–88, August 2011.

[151] Emily L Deer, Jessica González-Hernández, Jill D Coursen, Jill E Shea, Josephat Ngatia, Courtney L Scaife, Matthew A Firpo, and Sean J Mulvihill. Phenotype and genotype of pancreatic cancer cell lines. *Pancreas*, 39(4):425–35, May 2010.

[152] Jaroslaw Baran, Monika Baj-Krzyworzeka, Kazimierz Weglarczyk, Rafal Szatanek, Maria Zembala, Jakub Barbasz, Antoni Czupryna, Antoni Szczepanik, and Marek Zembala. Circulating tumour-derived microvesicles in plasma of gastric cancer patients. *Cancer immunology, immunotherapy : CII*, 59(6):841–50, June 2010.

[153] Wenjie Wang, Huiyu Li, Zhou Yan, and Jie Shenghua. Peripheral blood microvesicles are potential biomarkers for hepatocellular carcinoma - Cancer Biomarkers - Volume 13, Number 5 / 2013 - IOS Press. *Cancer Biomarkers*, 13(5):351–357, 2013.

[154] P C W Davies and C H Lineweaver. Cancer tumors as Metazoa 1.0: tapping genes of ancient ancestors. *Physical biology*, 8(1):015001, February 2011.

[155] Rob A Cairns, Isaac S Harris, and Tak W Mak. Regulation of cancer cell metabolism. *Nature reviews. Cancer*, 11(2):85–95, February 2011.

[156] Weiqin Lu, Helene Pelicano, and Peng Huang. Cancer metabolism: is glutamine sweeter than glucose? *Cancer cell*, 18(3):199–200, September 2010.

[157] Kristin F. Wilson, Jon W. Erickson, Marc A. Antonyak, and Richard A. Cerione. Rho GTPases and their roles in cancer metabolism. *Trends in Molecular Medicine*, 19(2):74–82, 2013.

[158] Michael J Lukey, Kristin F Wilson, and Richard A. Cerione. Therapeutic strategies impacting cancer cell glutamine metabolism. *Future medicinal chemistry*, 5(14):1685–700, October 2013.

[159] Darren J Burgess. Glioblastoma: Microvesicles as major biomarkers? *Nature reviews. Cancer*, 13(1):8, January 2013.

[160] J Nilsson, J Skog, A Nordstrand, V Baranov, L Mincheva-Nilsson, X O Breakefield, and A Widmark. Prostate cancer-derived urine exosomes: a novel approach to biomarkers for prostate cancer. *British journal of cancer*, 100(10):1603–7, May 2009.

[161] Seon Hee Kim, Nicole Bianco, Rajasree Menon, Eric R Lechman, William J Shufesky, Adrian E Morelli, and Paul D Robbins. Exosomes derived

from genetically modified DC expressing FasL are anti-inflammatory and immunosuppressive. *Molecular therapy : the journal of the American Society of Gene Therapy*, 13(2):289–300, February 2006.

[162] Roberta Valenti, Veronica Huber, Manuela Iero, Paola Filipazzi, Giorgio Parmiani, and Licia Rivoltini. Tumor-Released Microvesicles as Vehicles of Immunosuppression. *Cancer Research*, 67(7):2912–2915, April 2007.

[163] Lucia Mincheva-Nilsson and Vladimir Baranov. The role of placental exosomes in reproduction. *American journal of reproductive immunology (New York, N.Y. : 1989)*, 63(6):520–33, June 2010.

[164] Rebecca A Dragovic, Christopher Gardiner, Alexandra S Brooks, Dionne S Tannetta, David J P Ferguson, Patrick Hole, Bob Carr, Christopher W G Redman, Adrian L Harris, Peter J Dobson, Paul Harrison, and Ian L Sargent. Sizing and phenotyping of cellular vesicles using Nanoparticle Tracking Analysis. *Nanomedicine : nanotechnology, biology, and medicine*, 7(6):780–8, December 2011.

[165] Richard Wubbolts, Rachel S. Leckie, Peter T. M. Veenhuizen, Guenter Schwarzmann, Wiebke Mobius, Joerg Hoernschemeyer, Jan-Willem Slot, Hans J. Geuze, and Willem Stoorvogel. Proteomic and Biochemical Analyses of Human B Cell-derived Exosomes: POTENTIAL IMPLICATIONS FOR THEIR FUNCTION AND MULTIVESICULAR BODY FORMATION. *J. Biol. Chem.*, 278(13):10963–10972, March 2003.

[166] Suresh Mathivanan, Justin W E Lim, Bow J Tauro, Hong Ji, Robert L Moritz, and Richard J Simpson. Proteomics analysis of A33 immunoaffinity-purified exosomes released from the human colon tumor cell line LIM1215 reveals a

tissue-specific protein signature. *Molecular & cellular proteomics : MCP*, 9(2):197–208, February 2010.

[167] Bow J Tauro, David W Greening, Rommel A Mathias, Hong Ji, Suresh Mathivanan, Andrew M Scott, and Richard J Simpson. Comparison of ultracentrifugation, density gradient separation, and immunoaffinity capture methods for isolating human colon cancer cell line LIM1863-derived exosomes. *Methods (San Diego, Calif.)*, 56(2):293–304, February 2012.

[168] David W Inglis, John A Davis, Robert H Austin, and James C Sturm. Critical particle size for fractionation by deterministic lateral displacement. *Lab on a chip*, 6(5):655–8, May 2006.

[169] Lotien Richard Huang, Edward C Cox, Robert H Austin, and James C Sturm. Continuous particle separation through deterministic lateral displacement. *Science*, 304:987–990, 2004.

[170] Nicole Pamme. Continuous flow separations in microfluidic devices. *Lab on a Chip*, 7(12):1644, November 2007.

[171] Jason P. Gleghorn, James P. Smith, and Brian J. Kirby. Transport and collision dynamics in periodic asymmetric obstacle arrays: Rational design of microfluidic rare-cell immunocapture devices. *Physical Review E*, 88(3):032136, September 2013.

[172] Martin Heller and Henrik Bruus. A theoretical analysis of the resolution due to diffusion and size dispersion of particles in deterministic lateral displacement devices. *Journal of Micromechanics and Microengineering*, 18(7):075030, July 2008.

[173] Kevin Loutherback, Kevin S. Chou, Jonathan Newman, Jason Puchalla, Robert H. Austin, and James C. Sturm. Improved performance of deterministic lateral displacement arrays with triangular posts. *Microfluidics and Nanofluidics*, 9(6):1143–1149, May 2010.

[174] Youlan Li, Colin Dalton, H John Crabtree, Gregory Nilsson, and Karan V I S Kaler. Continuous dielectrophoretic cell separation microfluidic device. *Lab on a chip*, 7(2):239–48, February 2007.

[175] Benjamin G Hawkins, A Ezekiel Smith, Yusef A Syed, and Brian J Kirby. Continuous-Flow Particle Separation by 3D Insulative Dielectrophoresis Using Coherently Shaped, dc-Biased, ac Electric Fields. *Analytical Chemistry*, 79:7291–7300, 2007.

[176] James V Green, Milica Radisic, and Shashi K Murthy. Deterministic lateral displacement as a means to enrich large cells for tissue engineering. *Analytical chemistry*, 81(21):9178–82, November 2009.

[177] Stefan H Holm, Jason P Beech, Michael P Barrett, and Jonas O Tegenfeldt. Separation of parasites from human blood using deterministic lateral displacement. *Lab on a chip*, 11(7):1326–32, April 2011.

[178] David W Inglis, Nick Herman, and Graham Vesey. Highly accurate deterministic lateral displacement device and its application to purification of fungal spores. *Biomicrofluidics*, 4(2):024109, January 2010.

[179] Giulia Taraboletti, Sandra D'Ascenzo, Ilaria Giusti, Daniela Marchetti, Patrizia Borsotti, Danilo Millimaggi, Raffaella Giavazzi, Antonio Pavan, and Vincenza Dolo. Bioavailability of VEGF in tumor-shed vesicles depends on vesicle burst induced by acidic pH. *Neoplasia (New York, N.Y.)*, 8(2):96–103, February 2006.

[180] M Skobe, T Hawighorst, D G Jackson, R Prevo, L Janes, P Velasco, L Riccardi, K Alitalo, K Claffey, and M Detmar. Induction of tumor lymphangiogenesis by VEGF-C promotes breast cancer metastasis. *Nature medicine*, 7(2):192–8, February 2001.

[181] S A Stacker, C Caesar, M E Baldwin, G E Thornton, R A Williams, R Prevo, D G Jackson, S Nishikawa, H Kubo, and M G Achen. VEGF-D promotes the metastatic spread of tumor cells via the lymphatics. *Nature medicine*, 7(2):186–91, February 2001.

[182] S-I Ishigami, S Arii, M Furutani, M Niwano, T Harada, M Mizumoto, A Mori, H Onodera, and M Imamura. Predictive value of vascular endothelial growth factor (VEGF) in metastasis and prognosis of human colorectal cancer. *British Journal of Cancer*, 78(10):1379–1384, November 1998.

[183] Alex Yuan, Erica L Farber, Ana Lia Rapoport, Desiree Tejada, Roman Deniskin, Novrouz B Akhmedov, and Debora B Farber. Transfer of microRNAs by embryonic stem cell microvesicles. *PloS one*, 4(3):e4722, January 2009.